Oceanic Forcing of the Wintertime Low-Frequency Atmospheric Variability in the North Atlantic European Sector: A Study with the ARPEGE Model

CHRISTOPHE CASSOU AND LAURENT TERRAY

Climate Modelling and Global Change Project, CERFACS/SUC URA 1875, Toulouse, France

(Manuscript received 19 January 2001, in final form 18 May 2001)

ABSTRACT

The relationship between global sea surface temperatures (SSTs) and the North Atlantic–Europe (NAE) atmospheric circulation is investigated using an ensemble of eight simulations with the ARPEGE atmospheric global circulation model forced with prescribed SSTs over the 1948–97 period. The model mean state is first validated against NCEP reanalyses. The interannual SST-forced variability is then compared to the internal one using analysis of variance (ANOVA) techniques. Both components are maximum in winter over the Northern Hemisphere and the associated potential predictability shows weak but significant values located over the Icelandic low (IL) and the Azores high (AH).

The North Atlantic oscillation (NAO) is found to be the leading internal variability mode over the NAE sector as shown by principal component analysis of a control simulation with climatological SSTs. The noise imprint dominates the forced response estimated from the ensemble mean. The latter is related first to the El Niño–Southern Oscillation (ENSO) activity. During warm (cold) events in the Pacific, the AH shows negative (positive) pressure anomalies and weakened opposition with the IL. The AH fluctuations exhibit a 3.7-yr peak and result from changes in the activity of the Atlantic Hadley cell and from the eastward extension of the Pacific North America teleconnection pattern. Eliassen–Palm diagnostics show that eddy–mean flow interaction acts to maintain the anomalous Atlantic stationary wave pattern as described by Fraedrich in a review based on observational results. The simulated ENSO–NAE connection is, however, too strong in the model and this dominance may be related to the simulated mean state biases. Second, the North Atlantic atmospheric forced signal is associated with the Atlantic SSTs. A tripole structure over the North Atlantic basin with maximum loading in its tropical branch is linked to the phase of the simulated NAO. A local Hadley cell mechanism associated with Rossby wave excitation over the Atlantic is suggested to explain tropical–midlatitude interactions in the model.

1. Introduction

Global mean surface temperature has risen about 0.3°–0.6° since the late nineteenth century (Houghton et al. 1995). Most of the warming occurs over land in the Northern Hemisphere, especially over the northern Eurasian continent and less importantly over the western central flank of North America. Concurrent surface anomalies in rainfall and storminess link the temperature increase to changes in global atmospheric circulation especially in winter. Hurrell (1996) reported that the recent temperature trend is tightly related to the modification of large-scale climate variability modes. The alteration in the occurrence and the persistence of the El Niño–Southern Oscillation (ENSO) and the North Atlantic oscillation (NAO) projects remarkably well onto the observed climate trend. ENSO couples west–east equatorial pressure changes over the tropical Pacific with the sea surface temperature (SST) fluctuations between warm (El Niño) and cold (La Niña) anomalies over the central-eastern equatorial Pacific. It is known to have a global influence (Halpert and Ropelewski 1992) either via standing modes over the entire Tropics or via coherent large-scale low-frequency spatial patterns referred to as ''teleconnections'' over midlatitudes (see Wallace and Gutzler 1981 for a review).

The NAO has been first described by Walker (1924) and may be viewed as the Atlantic mark of a larger hemispheric mode referred to as Arctic oscillation in Thompson and Wallace (1998). It affects the meridional mass balance between the Icelandic low (IL) and the Azores high (AH) leading to pronounced regional changes over the entire North Atlantic–European (NAE) domain downstream across to Asia. The NAO reveals a marked trend toward a persistent positive phase (deeper IL, stronger AH). This yields mild winters in Europe extending eastward up to western Siberia, severe ones over the northeastern Canada and the northwest Atlantic (van Loon and Rogers 1978 and references therein), and changes in sea-ice cover over the Labrador and Greenland Seas (Kwok 2000). Associated with the modification in the intensity and preferred track of the synoptic

Corresponding author address: Dr. Christophe Cassou, Climate Modelling and Global Change Project, CERFACS/SUC URA 1875, 42 ave. G. Coriolis, Toulouse 31057, France.
E-mail: cassou@cerfacs.fr

storms, a meridional precipitation dipolar structures covers most of Europe (Hurrell 1995), contrasting wet winters over the northern part of the Eurasian continent and persistent droughts over most of the Mediterranean countries up to the Middle East. Dominant in the 1960s and the 1970s, the negative phase (weaker IL/weaker AH) shows fairly symmetrical signals both in surface temperature and rainfall (Terray and Cassou 2000). The mean flow exhibits a slight southward shift concurrent with preferred zonal storm tracks heading toward France and Portugal (Serreze et al. 1997).

The relationship between ENSO and NAO is very controversial. Fraedrich (1994) in a study based on a century-long European record confirms the equatorial Pacific–North Atlantic association via the extension of the Pacific–North American (PNA) variability mode (Wallace and Gutzler 1981), while Huang et al. (1998) found an opposite phase relationship. More recently, Rodo et al. (1997) reported some statistical relationships between rainfall over Spain and ENSO activities. On the other hand, Rogers (1984) clearly denies any connection between the NAO and ENSO in agreement with some modeling studies (Kang and Lau 1986). The NAO–ENSO relationship is still an ongoing question. It may be well dependent on the strength and the sign of the Pacific episodes as it may strongly rely upon nonlinear processes. It may also experience decadal fluctuations through interaction with the midlatitude North Pacific and/or the tropical Atlantic Ocean. Improved understanding of these two main variability modes as well as their connection is essential to assess the likely range of future climate fluctuations and the extent to which these fluctuations are predictable. Detailed knowledge of the so-called natural variability is a necessary prerequisite to determine the origin of the recent changes and in particular to assess the potential impact due to anthropogenic forcing.

Our knowledge of the processes governing the NAO is still limited. This is partly explained by the nature of the variability over midlatitudes, which is not only forced by the SST fluctuations (Lau 1997), but primarily excited by the internal dynamics of the atmosphere. While ENSO is a large-scale coupled ocean–atmosphere tropical phenomenon, the midlatitude low-frequency patterns may result from complex aggregations and mutual influences of a wide range of weather–climate variations. These involve energy transfers between different scales of motion (Stephenson et al. 2000), thus introducing a high level of unpredictability. The relative weight between this ''noise'' and the deterministic signal referring to the ''SST-forcing'' as well as their interaction, is a key issue for better understanding interannual to decadal variability. Quantifying the level of the former and identifying its signature appear to be a necessary prerequisite to the detection of the latter.

The spectrum of the NAO time series displays energy concentration at interannual to decadal frequencies centered at 2.8 yr and between 6 and 8 yr (Hurrell and van Loon 1997). The influence of external forcings explaining higher loading in the low-frequency band is suggested, even if record length might be too short to assess robust conclusions (Wunsch 1999). Various deterministic mechanisms have been proposed involving for instance the coupling with the stratosphere through vertical propagating planetary waves (Perlwitz and Graf 1995) or the interaction between the atmospheric flows and the oceanic variability. There are clear indications that the North Atlantic Ocean covaries with the overlying atmosphere. For instance, it has been shown that the SSTs are responding to the atmosphere forcing on monthly to seasonal timescales (Frankignoul et al. 1998). In a review, Frankignoul (1985) reports that the SST variability tends to lag by a month or two the surface pressure/wind anomalies. Bladé (1997) reaches a similar conclusion using an atmospheric global circulation model (AGCM) coupled to an oceanic mixed layer model. The central question is the existence of the SST feedback onto the atmosphere, since once generated, SST anomalies are likely to persist long enough to affect in turn the atmospheric circulation. Some studies (Bladé 1997; Saravanan and McWilliams 1997; Saravanan 1998) find evidence of local thermal air–sea interactions that act to dampen surface heat flux variability.

While there is observational-cum-modeling evidence of significant atmospheric forcing on the underlying SSTs, it is of great interest to consider the possible reverse active influence of oceanic surface conditions in shaping midlatitude atmospheric variability. The important role played by tropical SST anomalies in forcing teleconnection patterns over the North Pacific American (NPA) domain (Horel and Wallace 1981) is widely recognized through the Rossby wave mechanism (Hoskins and Karoly 1981). By contrast, the potential forcing role of the ocean over the NAE atmospheric fluctuations is less clear. In a forced atmospheric context, the impact of Atlantic SST anomalies onto the NAE atmospheric variability has been suggested (Rodwell et al. 1999; Venske et al. 1999). Artificially amplified SST anomalies located in the North Atlantic midlatitude Ocean are generally prescribed in the model atmosphere (Palmer and Sun 1985; Kushnir and Held 1996) to investigate the atmospheric response. The latter reference shows a baroclinic vertical disturbance in the atmosphere downstream of the anomalous SST pattern, with a phase relationship between the low-level atmospheric and oceanic surface changes. The former one isolates an equivalent barotropic signature related to the prescribed midlatitude oceanic anomalies. Similar conclusions are found in Peng et al. (1995), but this study emphasizes the lack of reproducibility of the atmospheric changes. There is a large scatter in the responses of atmospheric models to SST anomalies, depending on the model physics and resolution, the basic mean state or the structure of the SST anomalous patterns. Indeed, applying large SST anomalies should call for caution since most of the

processes at work are strongly nonlinear and thus may be sensitive to the magnitude of the oceanic perturbations. In a coupled context, Latif and Barnett (1994) have reported a strong midlatitude atmospheric response to underlying SST anomalies, arguing for the existence of unstable air–sea interactions.

In the light of such a disparity in model results, we have conducted a series of experiments using the ARPEGE AGCM in order to quantify and characterize the fraction of the North Atlantic variability that is fully determined by a prescribed observed SST, without any a priori knowledge of the particular SST anomaly structure and magnitude creating the atmospheric response. Our goal is to isolate the spatiotemporal structure of the oceanic anomalies that has the strongest link to the midlatitude tropospheric flow in the model over the NAE sector. A similar study is carried out from observed and reanalysis data to assess the degree of realism of the simulated atmospheric behavior. The SST-forced signal is traditionally investigated using ensemble simulations of AGCMs forced with observed SSTs and Sea Ice extents (SIEs) for multidecadal periods (see, e.g., Harzallah and Sadourny 1995; Rodwell et al. 1999). The main measure characterizing the SST influence is the spread (weak influence) or reproducibility (strong influence) between the different members of the ensemble. Robust conclusions require a large number of simulations as reported in Mehta et al. (2000) or sophisticated techniques to avoid the so-called noise contamination problem as described in Venske et al. (1999).

The paper is organized as follows. The model and experimental design are first presented in section 2. A quick overview of the model's ability to simulate a realistic climatology is given in section 3 by comparison to the National Centers for Environmental Prediction (NCEP) reanalysis. As a first step, a seasonally stratified analysis of the potential predictability (PP) has been carried out using the analysis of variance (ANOVA) method for the mean sea level pressure (MSLP), in order to quantify the relative weight between the atmospheric response due to SST anomalies and the one related to internal processes. Results will be described in section 4 with some additional comments on the model's skill in representing the observed variability. In view of ANOVA conclusions, subsequent sections analyze into more details the modeled wintertime North Atlantic variability and its relationship with the global SST anomalies using singular value decomposition (SVD) and composite charts. Emphasis is first laid in section 5 on the representation of the winter NAO and its link to both Pacific and Atlantic SSTs. Section 6 details the impact of the ENSO phase over the North Atlantic–Europe climate in the model. Some prevailing mechanisms are suggested involving the representation of the stationary waves and the transients as well as their interaction with the mean flow. Section 7 is devoted to the Atlantic SST influence on the NAE climate. Section 8 gives conclusions, open issues, and perspectives.

2. Model description and experimental setup

The AGCM used in this study is the third version of the ARPEGE-Climat model developed at Météo France from the ARPEGE/IFS operational weather prediction model jointly maintained by Météo France and the European Centre for Medium-Range Weather Forecasts. The ARPEGE model is a spectral model and uses a two time level semi-Lagrangian scheme with semi-implicit time discretization of the equations. The standard configuration of the climate version employs a T63 triangular horizontal truncation. Diabatic fluxes and nonlinear terms are calculated on a Gaussian grid of about 2.8° latitude by 2.8° longitude. The vertical is discretized over 31 levels (20 levels in the troposphere) using a progressive vertical hybrid coordinate extending from the ground up to about 34 km (7.35 hPa). The model time step for this resolution and time discretization scheme is 30 min.

ARPEGE includes all basic atmospheric physical parameterizations as well as comprehensive land surface processes via the ISBA model (Douville 1998). The deep convection is represented by a mass flux scheme with detrainment as proposed by Bougeault (1985). The stratiform and shallow convection cloud formation is evaluated via a statistical method described in Ricard and Royer (1993): the cloud-precipitation-vertical diffusion scheme follows turbulence properties to estimate the statistical water distribution at each grid point. The penetrative convection accounts for the vertical dependency of the air entrainment process (Terray 1998) and the closure condition is based on humidity convergence criteria. The radiative package follows the Fouquart and Morcrette scheme (Morcrette 1990). The longwave radiation parameterization includes the effect of trace gases (CH_4, N_2O, $CFC_{11–12}$) as well as CO_2, O_3, and H_2O. Parameterizations of boundary layer and turbulence are based on vertical exchange coefficients computed as functions of the local Richardson number according to the Louis et al.'s (1982) method.

A first 60-yr experiment has been performed with prescribed climatological annual cycle of monthly mean global SST and sea ice distribution. The SST and SIE climatologies are computed from a blend of two Global Sea Ice and Sea Surface Temperature (GISST) reconstructed datasets (Rayner et al. 1997); namely, the GISST 2.3 from 1947 to 1982 and the new released GISST 3.0 package from 1983 to 1998. This simulation is referred to as ''ACYC'' following the Lau and Nath (1994) nomenclature. An ensemble of eight multidecadal ''GOGA'' integrations has then been carried out using the same monthly dataset as boundary forcings. The global monthly mean SST and SIE fields have been interpolated using a Gaussian interpolation from their original grid ($1° \times 1°$) to the Gaussian grid of ARPEGE. Model grid boxes where ice cover exceeds 50% are considered as ice points. Each simulation starts on 1 January 1947 up to 31 March 1998, giving a set of 50

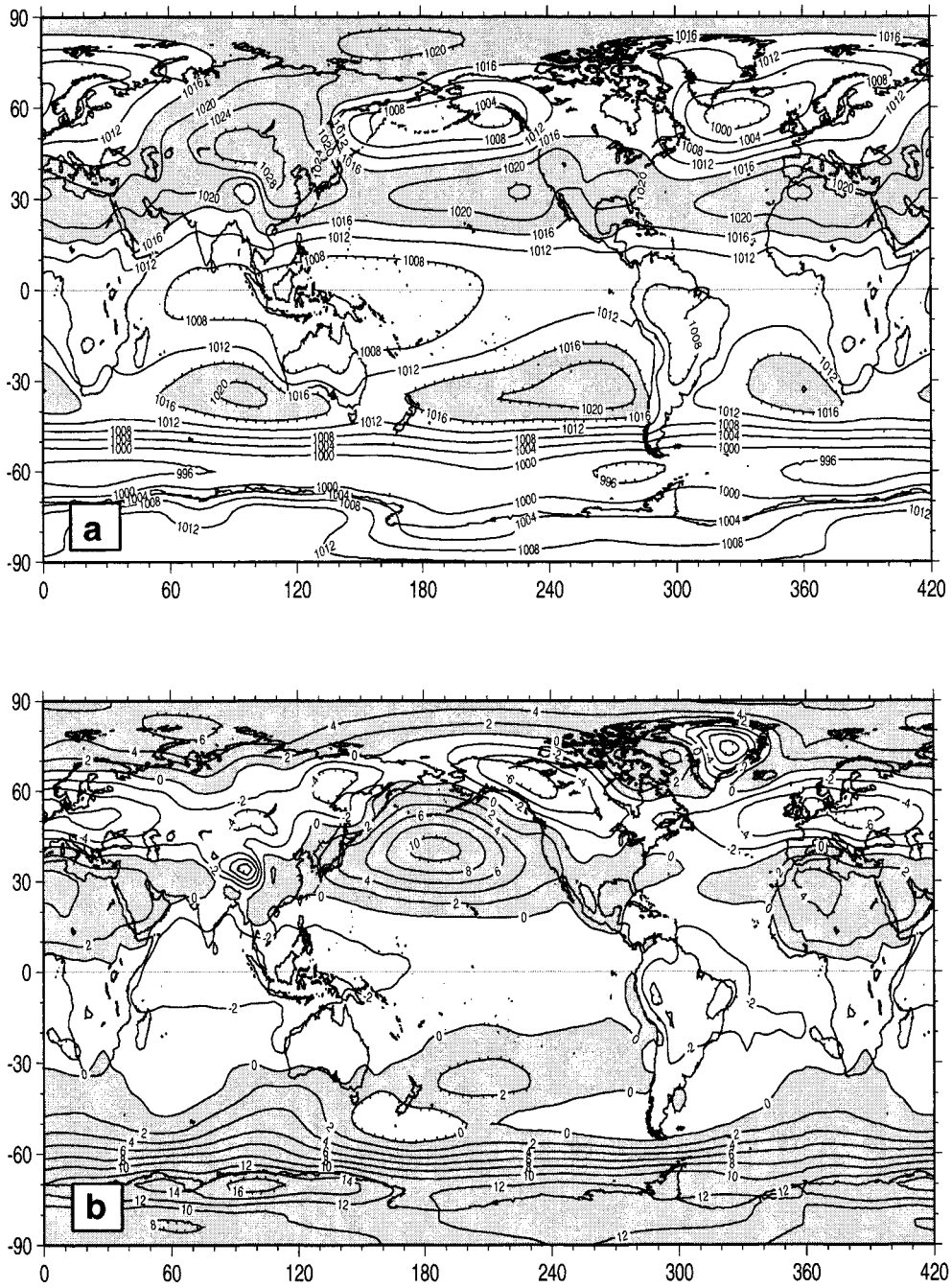

FIG. 1. (a) Dec–Feb (DJF) MSLP from ARPEGE and (b) differences from NCEP climatology. The contour interval in (a) is 4 hPa with shading above 1016 hPa. Differences are contoured every 2 hPa and shaded when positive.

complete years, the first simulated year being discarded in the subsequent analyses to account for the adjustment time of the land surface and atmospheric variables. The GOGA simulations differ only by their initial atmospheric conditions. These have been selected from late December states of the ACYC integration and are thus treated as independent estimates of the initial state of 1 January 1947. The CO_2 concentration is kept constant over the 50-yr integration and fixed to its 1990s value (353 ppmv; Houghton et al. 1995).

Dynamical simulated fields are compared to NCEP over the 1958–97 period. These have been downloaded from the LDEO Web site (http://ingrid.ldgo.columbia.edu/SOURCES/) (Kalnay et al. 1996).

3. Climatology

The purpose of this section is to briefly document the climatological behavior of the ARPEGE model. Much of the variability from interannual to decadal timescales is closely linked to the location and the intensity of the mean atmospheric features. The model's ability to reproduce them as well as their seasonal fluctuations thus appears essential. Model seasonal climatologies for dynamical fields are calculated based on monthly mean data over the 1958–97 period to be directly compared to NCEP after interpolation onto the model grid. Maps presented hereafter correspond to a given simulation among the 8-member ensemble. It has been verified that the climatology is not dependent on the selected experiment.

a. Mean sea level pressure

The simulated MSLP is traditionally validated against observation as it represents a vertically integrated measure of the model thermodynamic and dynamic skill. The distribution of the winter mean (Fig. 1a) shows an overall good agreement with reality. But in spite of substantial improvements comparing to earlier ARPEGE versions (Déqué et al. 1994), some biases remain and interestingly find some similarities with those described in Hurrell et al. (1998) for CCM3. The main deficiency of the model is found in the Pacific (Fig. 1b). The 30° northeastward shift of the Aleutian low center associated with the overestimated strength of the sinking branch of the Hadley cell yields errors as large as +10 hPa in the central basin and up to −6 hPa over Yukon. Over the Atlantic, the observed patterns and magnitudes are well simulated as the center of the IL is now well pined to the southern tip of Greenland compared to earlier versions of the model. However, the southwest–northeast pressure gradient over the eastern basin is still underestimated. This leads to a weak trough over northern Scandinavia and a too zonal distribution over western Europe. This feature is reinforced by the slightly overestimated high pressure ridge over North Africa related to the eastward extension of the AH. Note that the difference between observed and simulated MSLP over high topography (Greenland, the Himalaya, Antarctica, . . .) is not realistic due to sea level reduction calculation. Similar biases, with less intensity though, are found in the austral winter in the Southern Hemisphere with slightly too strong subtropical highs and too deep lows along the circumpolar belt (not shown). It is worth noting that the semi-Lagrangian scheme has considerably contributed in reducing the constant and important bias regarding the strength of the midlatitude southern lows.

b. Zonal wind at 200 hPa (U200)

The zonal wind component at 200 hPa is generally chosen to assess the model's ability to simulate the subtropical jet whose variations can lead to large changes in the stationary waves. For instance, Peng and Whitaker (1999) have emphasized the importance of the latitudinal and vertical positioning of the jet maxima to understand the atmospheric response to midlatitude SST changes. Figures 2a,b show, respectively, December–January–February (DJF) model's climatological mean and its difference with NCEP. The largest disagreements are found in the equatorial upper troposphere. A westerly bias over the western-central Pacific extending westward to the central Indian Ocean is associated with a too strong Walker cell. The latter results in an easterly bias west of the Andes, related to the strong subsidence around 240°E that enhances the convection over Amazonia. Midlatitude errors in the Northern Hemisphere are comparable to the tropical one. The dipole structure over the central North Pacific is related to the northward shift (by about 10° lat) of the subtropical jet leading to an easterly bias around 30°N and enhanced westerlies over the Aleutians. By contrast, the DJF Atlantic peak in the westerlies is in very good agreement with NCEP both in location and amplitude over the western basin and the east coast of the North American continent. But the simulated westerlies extend to far inland over Europe, consistently with the weakness of the north Scandinavian trough and the enhanced pressure gradient over the Mediterranean Sea described earlier. Over the Southern Hemisphere, the model is able to capture the zonal asymmetry with maximum westerlies over the Indian and Atlantic Oceans although it overestimates the strength of the westerlies throughout the entire latitude band. This is especially evident over New Zealand where the magnitude of the errors reaches 10 m s^{-1} during the austral summer.

c. Storm tracks

The term ''storm tracks'' usually refers to regions of preferred paths of the midlatitude synoptic eddies. These are characterized by a high day-to-day variability in MSLP or geopotential height and result from the baroclinic instability of the mean flow at such latitudes. Two main sectors of high baroclinicity can be found off the North American east coast and off the Japanese shore. These locations are set by the position of the subtropical jet and the maximum meridional low-level temperature gradient. The 3D perspective linking upper and lower troposphere is traditionally assessed by the 3D **E** vector defined as follows in pressure coordinates:

$$E_{3D} = (\overline{v'^2} - \overline{u'^2},\ -\overline{u'v'},\ -f_o\overline{v'\theta'}/\theta_p).$$

Here v, u, f_o, θ are standing, respectively, for the meridional wind, zonal wind, Coriolis force, potential temperature, and the prime ($'$) for their anomalies. The reader is invited to refer to Hoskins et al.'s (1983) study for a complete description of the **E** vector. The vertical component is represented by transient heat meridional flux

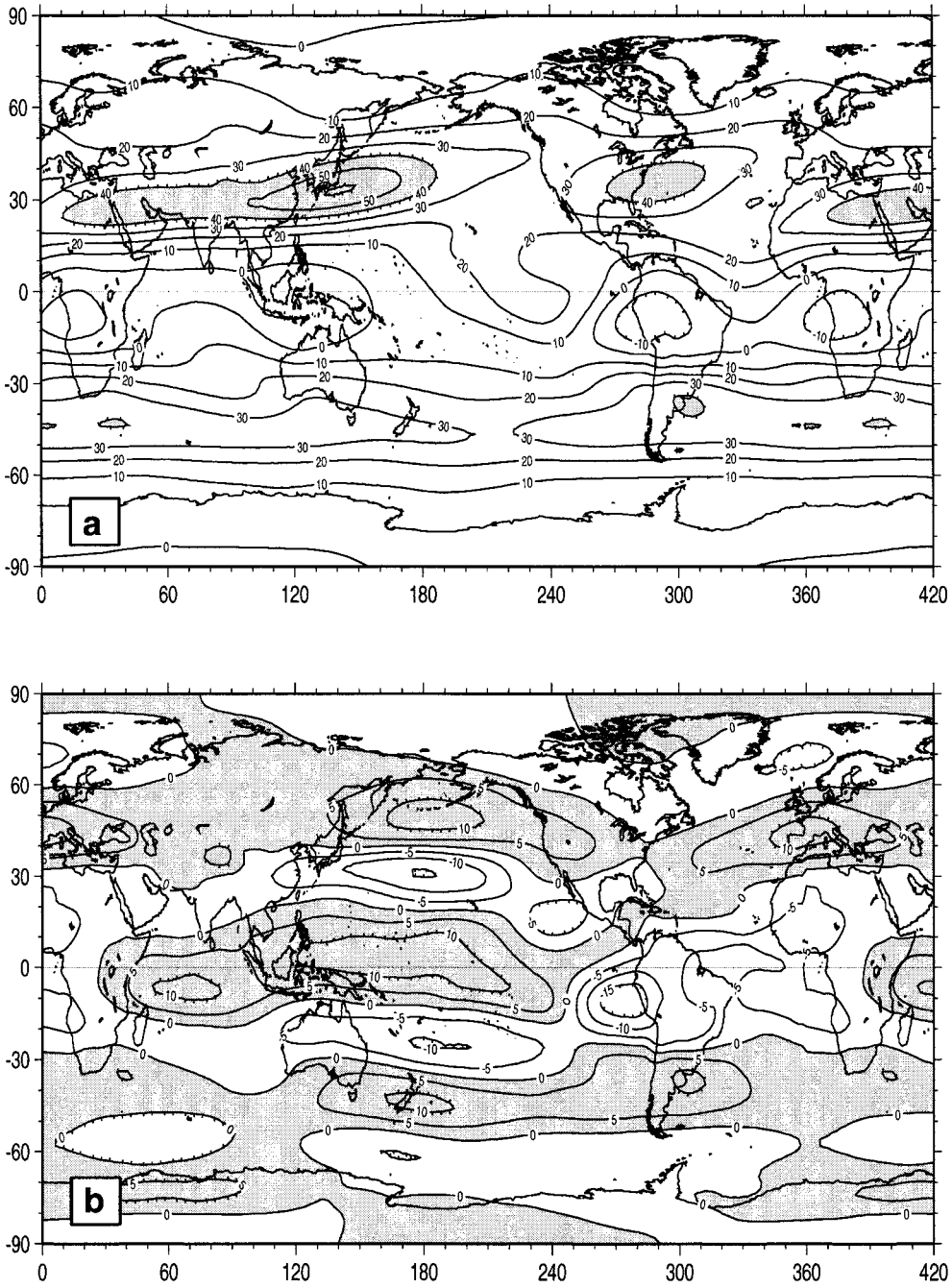

FIG. 2. (a) DJF U200 from ARPEGE and (b) differences from NCEP climatology. The contour interval in (a) is 10 m s^{-1} with shading above 40 m s^{-1}. Differences are contoured every 5 m s^{-1} and shaded when positive.

$\overline{v'T'}$ at 700 hPa while the horizontal ones are calculated at 200–250 hPa where maxima momentum transports occur. The divergence of the **E** vector is used to quantify the eddy feedback onto the mean flow. Divergence (convergence) of the upper-level momentum ($\overline{v'^2} - \overline{u'^2}$, $-\overline{u'v'}$) components indicates a positive (negative) feedback that thus tends to increase (decrease) the mean flow. The **E** vector is calculated on bandpass-filtered (2.2–6 days) daily data for the model and NCEP. Figure 3a shows its distribution over the Northern Hemisphere in DJF only for ARPEGE. The zonal asymmetry of the transient heat flux is well captured with maxima over the western part of both the Pacific and the Atlantic Oceans. The divergence of the upper-level vectors over these area shows the westerly forcing of the mean flow by the eddies. The most significant difference between the model and NCEP

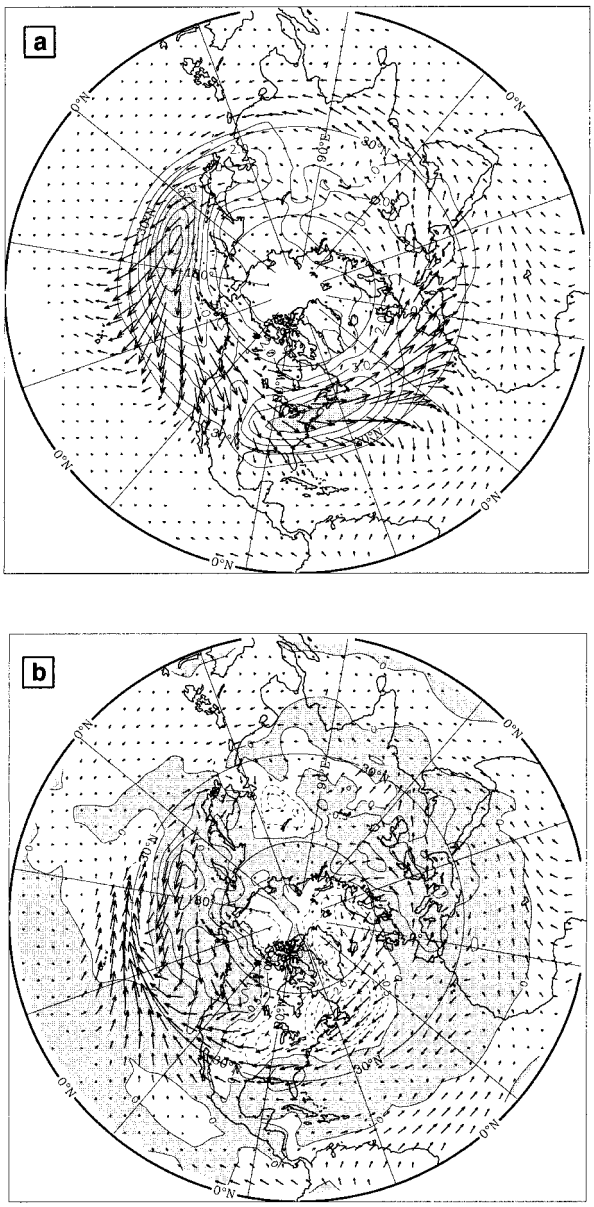

FIG. 3. Horizontal Eliassen–Palm 200-hPa vector superimposed on $\overline{v'T'}$ meridional heat transport by transient at 700 hPa calculated from 2.2–6-day bandpass-filtered daily data for DJF. (a) For the ARPEGE model, (b) for the differences from NCEP. The contour interval in (a) is 1 K m s^{-1} with shading above 5 K m s^{-1}. Differences are contoured every 0.5 K m s^{-1} and shaded when positive.

(Fig. 3b) appears over the North Pacific, where the storm track is too strong and extends too far poleward. This northward shift is consistent with earlier results on MSLP and U200 related to the Aleutian low. Over the Atlantic, the transient heat transport is clearly underestimated over Newfoundland although the opposite image shows up over Europe. The divergence of the upper vectors is shifted eastward and southward indicating that the eddies produce a too weak deceleration of the Atlantic subtropical jet at the downstream end of the storm track. This is in

TABLE 1. Skill and reproducibility of regional MSLP for the four traditional seasons. "Tropical" stands for average between 30°N/S, Northern (Southern) Hemisphere N (S) H between 0° and 90°N(S), North Pacific/North America over 30°–80°N, 120°–300°E, North Atlantic over 30°–80°N, 60°W–40°E. Columns 1 and 2 (σ) represent the MSLP variance in hPa unit of respectively, internal and SST-forced part, column 3 the PP in %. Column 4 (Area) stands for the percentage of surface where the PP is above the F test 95% significance limit. The skill of the model in reproducing the observed fluctuations is estimated via correlation (Corr). Boldface highlights maximum values among the four seasons.

	DJF				MAM				JJA				SON			
	MSLP variability				MSLP variability				MSLP variability				MSLP variability			
	σ_{SST}	σ_{INT}	PP	Area	Corr	σ_{SST}	σ_{INT}	PP	Area	Corr	σ_{SST}	σ_{INT}	PP	Area	Corr	σ_{SST}	σ_{INT}	PP	Area	Corr
Global	**0.7**	**5.3**	**26.4**	**74.6**	**0.28**	0.4	3.8	23.2	67.6	0.22	0.7	3.2	**26.4**	59.2	0.23	0.6	3.4	25.8	47.3	0.25
Tropics	**0.3**	0.3	**53.1**	99.4	**0.50**	0.2	0.2	49.6	99.3	0.44	**0.3**	**0.4**	47.3	**100.**	0.43	**0.3**	0.3	51.7	99.3	0.48
N/H	1.3	**10.3**	13.1	**69.1**	**0.16**	0.4	5.8	8.6	39.2	0.08	0.3	2.2	**14.8**	59.1	0.11	0.3	4.9	10.7	47.3	0.07
S/H	0.4	4.3	15.3	56.1	0.20	0.5	5.0	14.1	69.5	0.16	**1.5**	**7.0**	**19.0**	**93.7**	0.18	0.9	4.8	17.8	82.2	**0.23**
North Pacific/North America	**1.6**	**9.2**	15.5	**82.4**	**0.15**	0.5	5.4	10.6	45.4	0.07	0.3	2.2	**18.7**	71.1	0.13	0.4	4.6	11.4	52.2	0.11
North Atlantic	**1.3**	**12.8**	10.6	**55.3**	**0.17**	0.4	6.9	7.5	41.4	**0.17**	0.3	2.4	**12.3**	55.2	0.11	0.4	5.2	12.0	46.4	0.02

agreement with the too strong zonal jet over Europe noted in the previous section (Fig. 2b). Midlatitude errors in the precipitation rate (Cassou 1999) are clearly linked to the storm tracks misrepresentation with enhanced precipitation along the northward shifted storm path in the Pacific and overestimated rainfall over western Europe by a factor of 1.5.

4. Internal variability versus oceanic forcing

Quantifying the relative importance of the externally forced atmospheric variability versus the one caused by purely internal processes is assessed using the traditional analysis of variance often referred to as ANOVA technique and widely discussed in literature (see, e.g., Stern and Miyakoda 1995; Zwiers 1996; Senazzi et al. 1996). This statistical tool is based in its simplified form on the partition of the total variance of a given field into two independent components: the externally forced variability (associated with the prescribed SSTs and SIEs in our case) and the chaotic variability generated internally by the model. The ratio of these two components defines the PP. Many hypotheses are necessary to perform such a variance decomposition (Zwiers 1987). All the assumptions and the algorithm are thoroughly detailed in Rowell et al. (1995) to which the reader is referred for an exhaustive description of the method. The interaction between internal and external variability is generally neglected in ANOVA studies. This assumption is definitely the strongest since it is likely that the persistence of surface (land + ocean) processes may have a significant impact on the internal variability. In addition, due to the finite number of ensemble members, the externally forced variability part is still contaminated by the atmospheric noise (Venske et al. 1999). Indeed, it is approximated by the ensemble mean of a finite number of integrations and is therefore a biased estimate of the ''true'' forced response.

The impact of the oceanic forcing on the interannual timescale is investigated from seasonal means for the MSLP. Preliminary statistical tests have been applied to validate the method assumptions. A Kolmogorov–Smirnov test indicates that 99% of grid points pass the 95% significance limit and therefore verify the Gaussian distribution of the MSLP variability. An F test is applied between the atmospheric noise distribution extracted from the ensemble of GOGA integration and the variability given by the ACYC simulation. The idea here is to test the null hypothesis that the internal variance estimated from the ensemble through the ANOVA method is not significantly different than the true one estimated from ACYC. Results (not shown) interestingly highlight that it is not statistically possible to distinguish one distribution from the other except above high elevation areas (the Himalaya, Andes, and Kamtchatka Peninsula). This only represents 2% of the total grid points and this small percentage confirms the validity of the partition hypotheses.

Figure 4 displays the estimated fraction of total variance explained by the SST–SIE forcing (PP) for the four seasons defined as DJF, MAM, JJA, and SON means. It is not surprising to note high ratios over the Tropics (see, e.g., Moron et al. 1998) where the SST forcing is dominant. Maximum PP over the tropical band occurs during DJF (Fig. 4a) with peaks as high as 75% over the Atlantic Ocean, northwestern (15°N), and eastern equatorial Pacific. These features are clearly related to ENSO as depicted by a simple teleconnection analysis (not shown) based on correlations as in Wallace and Gutzler (1981). In the Southern Hemisphere, the SST–SIE-forced variance drops suddenly beyond 40°S. The strongest evidence of PP in the Northern Hemisphere extratropics is found over the oceans, even if values are rather low. A significant 20% core covers the whole Pacific with some extension over Alaska. The North Atlantic sector is more chaotic with no predictability over a broad croissant from Greenland to Russia in contrast to Davies et al.'s (1997) results. Note however in Fig. 4a, that the centers of action related to the NAO are significantly influenced by the SST forcing even if the values are quite small. The MAM distribution (Fig. 4b) is more consistent with previous studies (see, e.g., Brankovic et al. 1994) over the Pacific Ocean where maximum PP is found related to the strongest tropical-extratropical teleconnection. No significant changes compared to DJF are noted over the Atlantic Ocean even if the significance limit tends to extend about 10° northward and the minimum of PP is now centered over Iceland. During JJA (Fig. 4c), the ANOVA decomposition yields similar results in the Tropics and increased PP over the midlatitude of the Southern Hemisphere. In the Northern Hemisphere, maximum SST–SIE forcing appears over the North American continent whereas minimum values are found over the North Pacific Ocean. The opposite happens in the Atlantic with a local minimum over most of the European continent and higher values over the ocean with a 10%–15% band over the western and north basin. SON (Fig. 4d) suffers from very low levels of predictability beyond 30°N, while the tropical oceans are covered by the largest values especially over the Indian Ocean. This is the season of the greatest ENSO-related impacts in the Tropics that are partly phase-locked with the annual westward extension of the equatorial upwelling.

Further evidences of the seasonality in the strength of the oceanic forced component are summarized in Table 1. The MSLP variability both internal and external is the highest in boreal (austral) winter over the Northern (Southern) Hemisphere with maximum values in DJF on a global scale. Whereas the two components of the variability are the greatest in this season, the PP is found to be the strongest in JJA, except for the tropical band. Even though the SST-forced variability decreases significantly from winter to summer, very low values of the internal component have greater impact on the variance ratio. It would suggest that even if the SST-forced atmospheric fluctuations are definitely weaker, these might be easier to identify and might have a significant

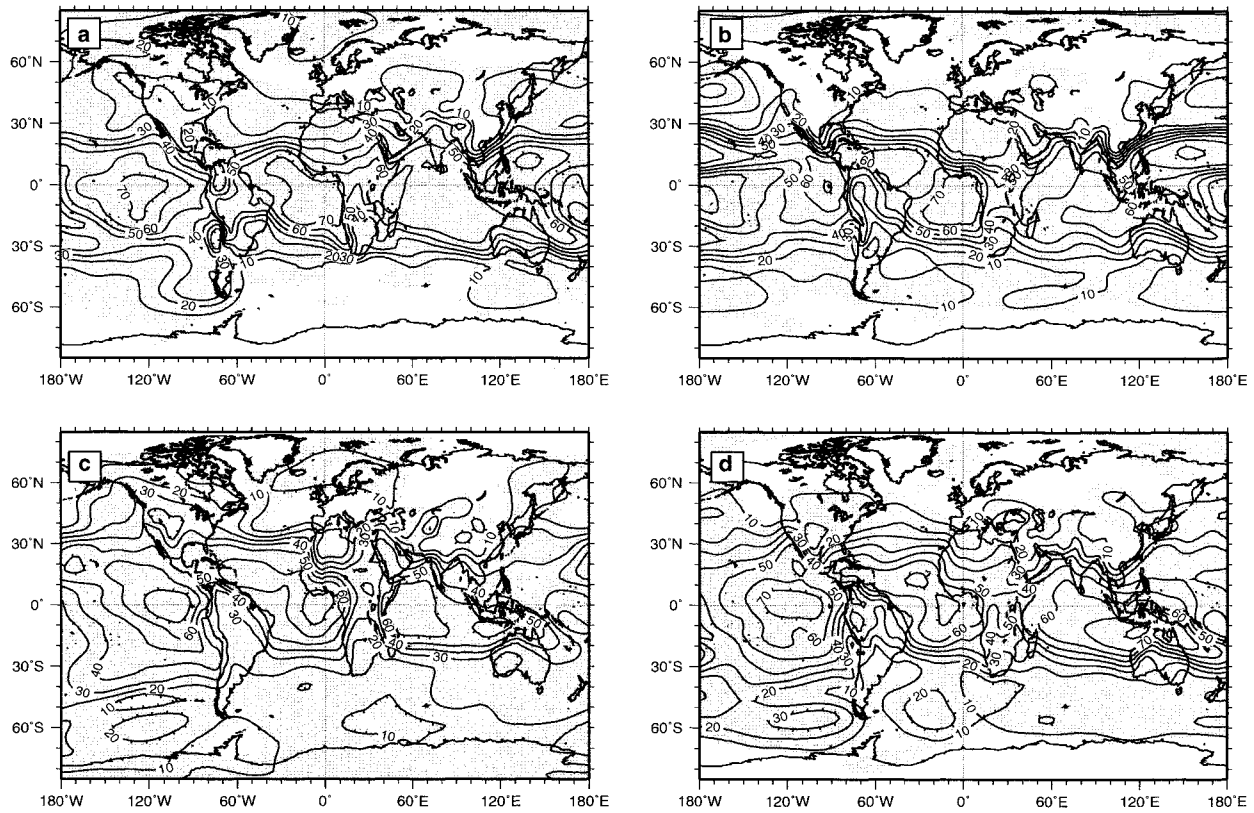

FIG. 4. Percentage of the variance of seasonal MSLP due to oceanic forcing. Results for each standard season (a) DJF, (b) MAM, (c) JJA, (d) SON are shown. The contour interval is 10% and white areas represent domains which fail the 95% significance limit estimated with an *F* test.

role in shaping the atmospheric JJA flow. However it is worth reminding that the box averaging process masks some important regionality. The most striking information from this table is the lack of predictability both in spring and vernal equinoxes over the midlatitudes.

The variance decomposition gives a first glimpse of the model behavior but is not sufficient to assess the skill of the model in simulating the observed variability. Evaluating its ability to reproduce the reality is achieved by computing a point-wise correlation between the model ensemble mean and the observations or reanalysis. The abbreviation ''corr'' in Table 1 refers to such a quantity. Maximum correlation occurs over the Tropics more precisely over the tropical Atlantic and Pacific Oceans (not shown), independently on the season. Weak or negative correlations are closely related to the main climatology biases even over regions where the PP is rather high (Indian Ocean) or clearly linked to areas of very low PP. These are indeed dominated by chaotic fluctuations, no matter how realistic the model response to SST changes is. This is the case over midlatitudes where maximum skill peaks at 0.17 and 0.23, respectively, for the Northern and Southern Hemisphere. These values are below the 95% confidence level based on a *t* test. Over the globe, maximum skill is diagnosed during DJF. Enhanced correlations are found both along the west coast of the North American continent in the Pacific as well as in Florida and southern Europe in the NAE sector.

Results on PP and model skill exhibit a strong seasonality. The balance between the competing external/internal sources is more favorable in boreal summer leading to the highest PP. On the other hand, the magnitude of both variabilities is rather weak compared to the others seasons. Thus boreal winters have been traditionally chosen to estimate the SST impact onto the atmosphere, even if the PP is slightly smaller. Mechanisms at work are clearly nonlinear and highly depend on the amplitude of the SST forced variability. In addition, teleconnections are known to be the most active both during the boreal winter and spring. Consequently, the rest of the paper will mostly concentrate on the DJF season over the NAE sector with some additional comments on MAM means.

5. The winter North Atlantic oscillation simulated by ARPEGE

A wide range of approaches has been applied in the literature to characterize the atmospheric variability modes. The simplest and oldest one is to define an index (Bjerknes 1964; Hurrell 1995; Jones et al. 1997) that

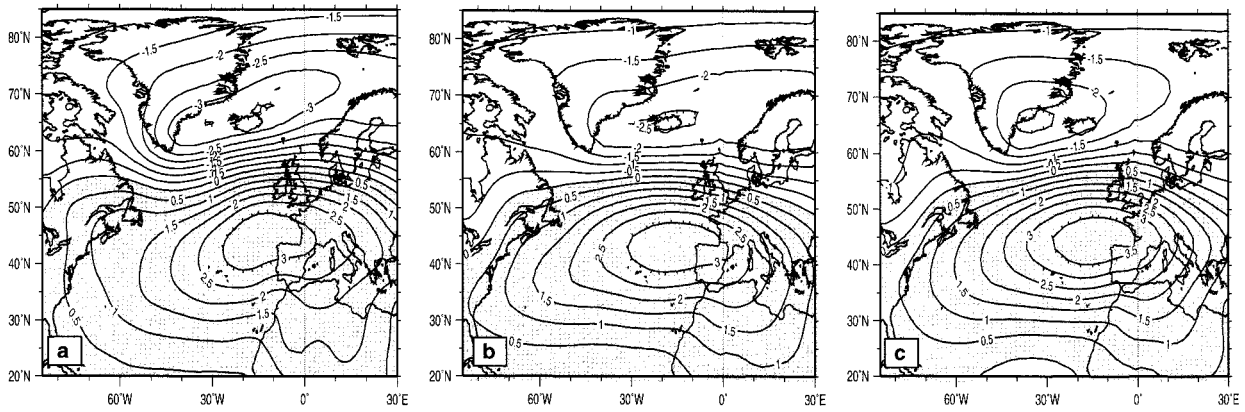

FIG. 5. Spatial pattern of the first MSLP EOF of the temporal covariance matrix for winter over the NAE sector for (a) NCEP, (b) GOGA, and (c) ACYC.

captures and summarizes the main physical characteristics of the variability structure. As described in Osborn et al. (1999), the NAO index (NAOI) can be either built on the normalized MSLP difference between weather stations close to the dipole centers or based on pattern analyses (Rogers 1990).

A standard empirical orthogonal function (EOF) of DJF MSLP data is performed over the NAE sector for the NCEP period (1959–98) in order to determine the centers of maximum variability. These will be chosen subsequently to build the model NAO index, to be compared to the observed one. Figures 5a,b,c, respectively, contrasts the leading EOF mode from NCEP with those obtained from one GOGA experiment and ACYC. The latter represents the internal atmospheric variability only, the former includes besides the SST-forced signal. EOF1 captures the NAO-like pattern in all of the datasets and accounts for the same amount of explained variance (about 50%). The observed dipolar structure estimated from NCEP is well represented by ARPEGE (Fig. 5b) both in terms of amplitude and location. The similarity between the GOGA and ACYC modes (Figs. 5b,c) is quite striking even if the IL remains slightly weaker and confined on the eastern Greenland coast in the latter. This confirms that the NAO is the dominant atmospheric mode over the NAE sector and mainly finds its origin in internal atmospheric processes (Saravanan 1998).

Whereas no discrepancies are found in the spatial structure of the NAO modes among the eight GOGA experiments, spectra associated with their principal components (PCs) exhibit significant deviations. Most of them as well as the one computed from the ACYC PC exhibit a flat spectrum characteristic of white noise processes; some of them share some redness with the NCEP PC. This shows that one has to be extremely cautions when interpreting one particular experiment.

As the model realistically captures the two main centers of action associated with the seesaw NAO mode, the traditional Azores minus Iceland normalized pressure difference is calculated for each GOGA experiments following Rodwell et al. (1999). It has been verified that a different calculation following Paeth et al. (1999) gives very similar results. The NAOI values of the eight individual model GOGA simulations show a wide dispersion (Fig. 6a), which is consistent with the weakness of the SST-forced signal as previously commented in the ANOVA section. In order to minimize the model noise influence, the ensemble mean hereafter referred to as GOGA-EM, is calculated and compared to the observed NAOI provided by the Center Research Unit, University of East Anglia (CRU–UEA), Norwich, United Kingdom (Jones et al. 1997). Their correlation is rather low (0.17) and fails the 95% level significance based on *t*-test statistics. The model simulates a quasi-permanent negative NAO phase in the 1950s, misses the pronounced decline in the 1960s, and underestimates the strong positive NAO phase in the 1990s. Mehta et al. (2000) have performed the same index construction using in their case, 16 GOGA atmospheric simulations. They found correlation values to be highly dependent on the number of runs used to compute the ensemble mean and, additionally, highly dependent on the simulations selected among the 16 when the NAOI is calculated on subsamples. Applying the same algorithm to the ARPEGE ensemble, the maximum coefficient correlation occurs with only four simulations retained for averaging, reaching a barely significant value at 0.31. This points out that the level of noise is highly dependent on the model and suggests that ARPEGE develops a strong internal variability that overcomes the forced signal.

The lag autocorrelation function shown in Fig. 6b emphasizes the weak persistence of the simulated NAO. Whatever the type of simulations considered here (individual realizations, ensemble mean, climatological ACYC run), the model lag autocorrelation drops significantly after 1 yr in contrast to UEA where persistence is still noticeable. Autocorrelation values above the significance threshold show up for GOGA-EM at 4 and 5

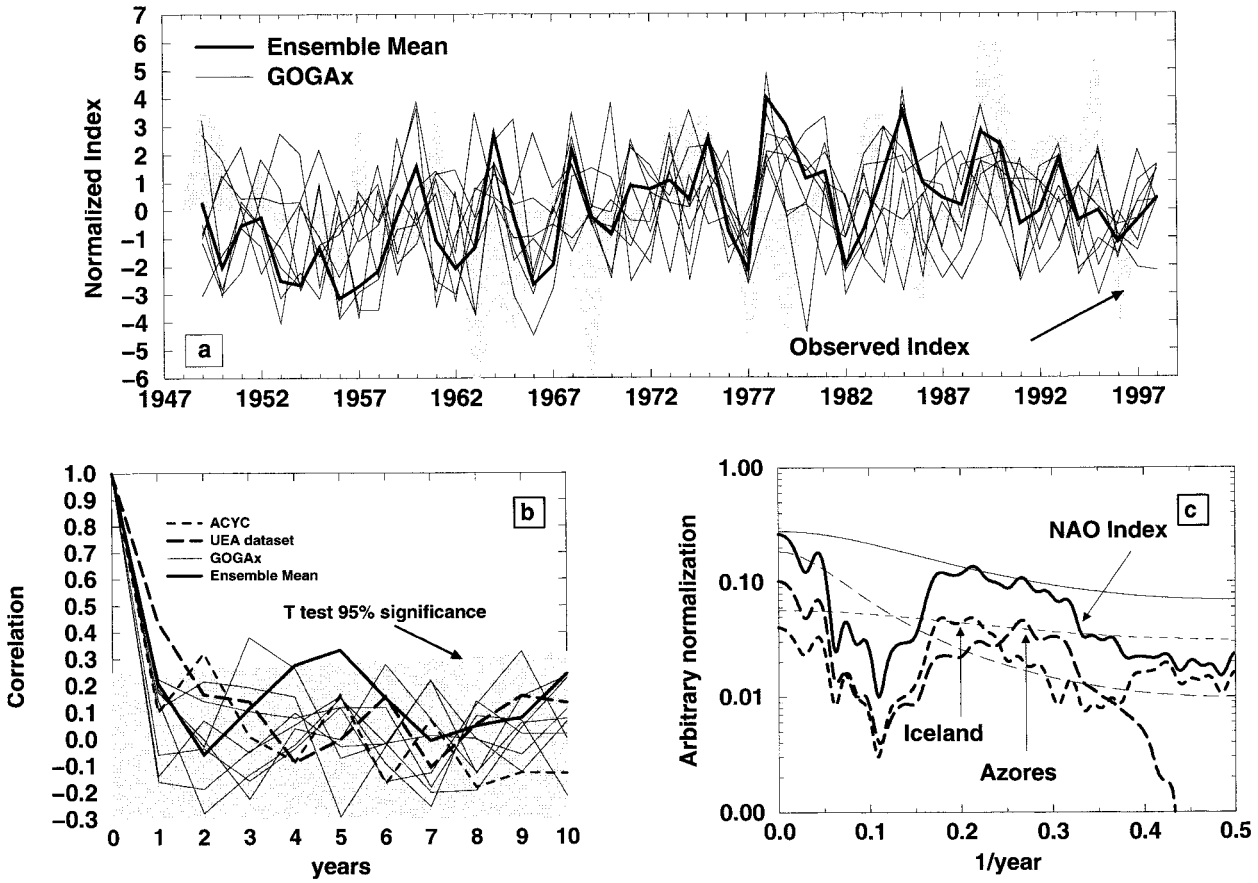

FIG. 6. (a) Normalized time series of the winter NAOI for observations (gray shading), each GOGA-type experiment (thin line), and the 8-member ensemble mean (heavy solid) from 1948 to 1998. (b) Winter-to-winter autocorrelation of the NAO index for individual GOGA experiments (thin line), for the ensemble mean (heavy solid), for NCEP (heavy dashed), and ACYC (thin dashed). (c) Multitaper spectral density estimate as a function of angular frequency of the ensemble mean NAO index and for the Azores and Iceland contribution. The 95% confidence intervals are estimated relatively to pure red noise [AR(1) process].

yr and may indicate a potential oscillatory behavior centered over this period. A spectrum analysis gives similar results (Fig. 6c). The NAOI spectrum for GOGA-EM is slightly red with energy concentration in the 3.5–5.5-yr band and in the trend. Barely significant peaks emerge around 5 yr and 3.7 yr. Whereas in reality the anticorrelation between the AH and the IL is rather high (-0.75 for UEA NAOI), it is generally underestimated in models. In the present case, the maximum found among the 8 members peaks at -0.68 whereas the minimum is as low as -0.39. Note that GOGA-EM anticorrelation reaches -0.61. Figure 6c emphasizes the dominant 3.7-yr signature in the Azores time series while the Icelandic variability is concentrated around 5 yr, their association leading to the broad peak of the classic model NAOI.

The global DJF SST is now regressed upon the Azores and Iceland indices considered separately in order to determine their respective link to oceanic conditions. The SST pattern associated with the IL (Fig. 7a) is dominated by large negative anomalies over the entire southern Atlantic basin concurrent with large positive anomalies north of 30°N centered off the Newfoundland coast. Smaller anomalies are found in between, the North Atlantic tropical part being mostly covered by positive SSTs with maximum values occurring off the Guyana coast. This spatial pattern resembles the first EOF SST mode calculated from the GISST dataset when the entire Atlantic basin is retained (not shown). Its link to the North Atlantic atmospheric variability has been suggested in Lau and Nath (1990, see their Fig. 4a). This mode can also be compared to the so-called South Atlantic interannual non-ENSO mode displayed in Mestas-Nuñez and Enfield (1999) using rotated EOF analysis. The SST structure related to the AH (Fig. 7b) exhibits a similar shape in the Atlantic. Some discrepancies appear however in the tropical band. Significant signals are now marginal in the southern Atlantic basin while anomalies in the northern part are reinforced. Above all, changes occurs in the equatorial Pacific, which exhibits a significant structure reminiscent of the ENSO mode.

To better confirm the link between ENSO and the

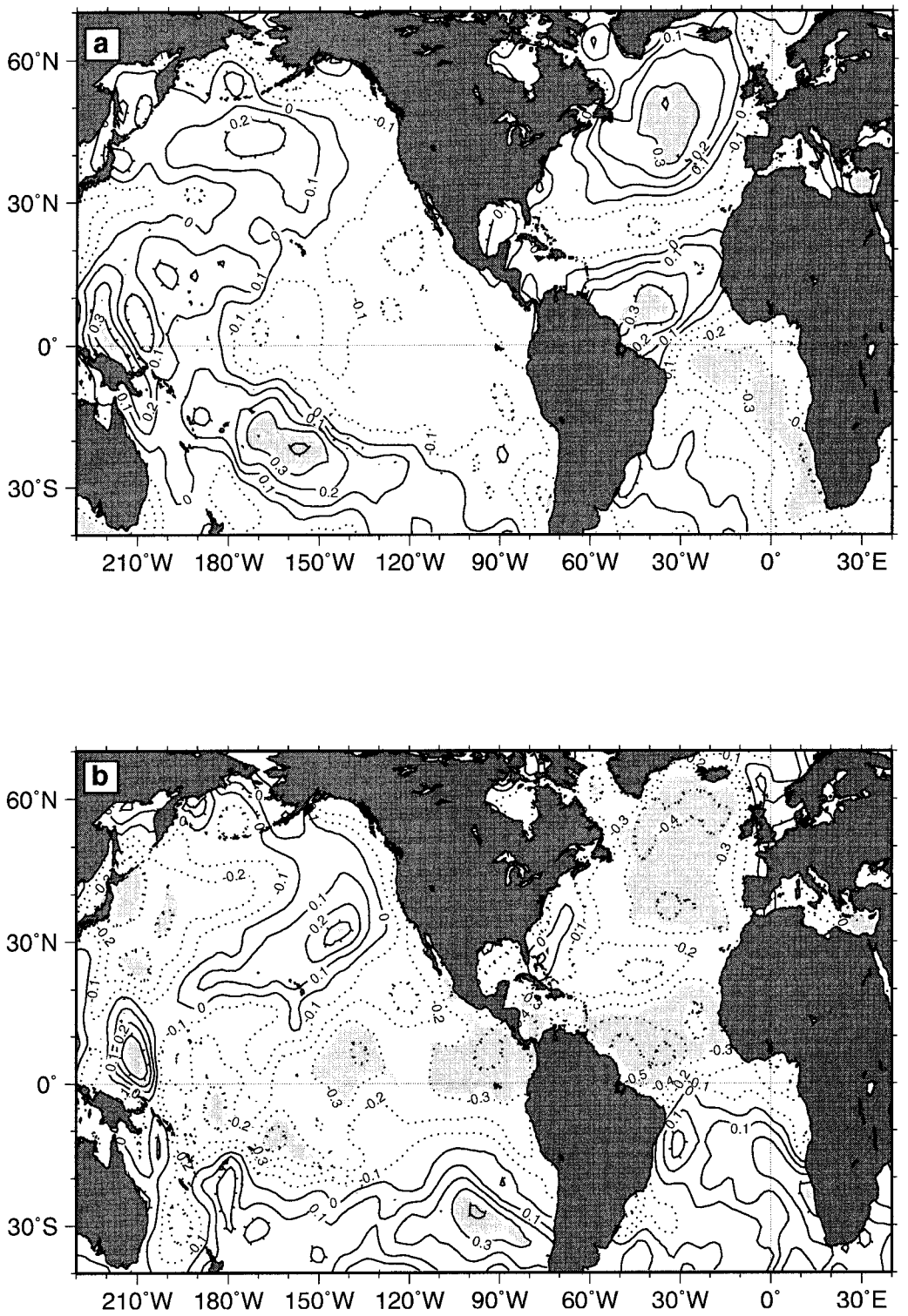

FIG. 7. Regression of the time series of the (a) GOGA-EM Iceland and (b) Azores indices onto the global GISST DJF SSTs. Shading stands for areas above the 95% significance limit based on a *t* test.

NAE atmosphere in the model, a maximum covariance analysis is performed using the SVD technique (Bretherton et al. 1992). The SVD analysis has been widely used in numerous studies (see, e.g., Wallace et al. 1992). It splits two fields into eigenmodes maximizing their cross covariance. Each pair of singular vectors is associated with their respective expansion coefficients and a squared covariance fraction. Confidence in SVD results requires a good serial correlation between the pair of expansion coefficients, a high fraction of covariance captured by the leading pairs, as well as their resemblance with the first modes obtained by EOF analysis. Statistical significance is assessed by a Monte Carlo approach as described, for instance, in Czaja and Frankignoul (1999) and Ward and Navarra (1997). It has been verified that all results presented thereafter are above the 95% significance level either based on the Monte Carlo approach for SVD decompositions or classic *t*-test statistics for correlations. The SST domain extends from 140°E up to the Pacific American coast in the 15°N–15°S belt while the MSLP area is restricted to the NAE (20°–85°N–80°W–35°E) sector. As the SVD technique assumes stationary time series, the linear trend is substracted in both MSLP and SST datasets over the NCEP period. The first covariant mode captures 94% of the total covariance. The pressure pattern shown in Fig. 8a exhibits a monopole centered slightly north of the Azores archipelago at roughly 47°N with some extension from Florida toward the Baltic Sea. It explains a small amount of the total variance and does not find its counterpart in observed data [the most similar pattern would be the so-called eastern Atlantic pattern defined for instance in Barston and Livezey (1987) but it misses all the secondary centers of action]. The SST pattern (Fig. 8b) associated with the MSLP mode reveals typical ENSO-related anomalies along the equatorial cold tongue in the Pacific. Time series (Fig. 8c) exhibit a strong correlation reaching 0.8. Since the model Pacific–North Atlantic (PNA) connection during ENSO episodes affects only the AH, it weakens the NAO coupling with the IL and may disrupt a potential link between the North Atlantic atmosphere and the underlying North Atlantic SST as suggested in Fig. 7. This might also be connected to the weaker anticorrelation between the AH and IL time series as detailed previously. Processes involved in the ENSO influence on the North Atlantic are now investigated in the following section.

6. ENSO impacts on the North Atlantic variability

a. Modeling the ENSO

The Southern Oscillation index (SOI) defined as the normalized pressure difference between Tahiti and Darwin, Australia, is commonly used as a simple measure of the seesaw equatorial pattern and provides a first-order diagnostic of the AGCM's skill in simulating the atmospheric response associated with warm and cold events. Figure 9 compares the simulated index of each individual GOGA experiment to the observed one calculated over the winter months (DJF) from the UEA dataset. The correlation between GOGA-EM and observed values reaches 0.75, which reflects the ability of ARPEGE in simulating the Pacific pressure anomalies related to ENSO forcing. Note however a slight overestimation of the SOI variability also found in recent modeling studies (Renshaw et al. 1998). The spread from one GOGA run to another is rather weak, correlations with observations ranging from 0.79 to 0.69 in agreement with the ANOVA conclusions especially for extreme events.

Interannual variability of the equatorial Pacific SSTs has been associated with persistent regional and global atmospheric anomalies designated as teleconnections and widely documented in literature based either on observational (see, e.g., Deser and Wallace 1990; Halpert and Ropelweski 1992; Livezey and Smith 1999) or modeling studies (e.g., Bladé 1999; Lau and Nath 1994). A detailed review is given by Trenberth et al. (1998) where they address roles and mechanisms of tropical–extratropical interactions. In the previous section, it has been shown that the ENSO events affect the model NAE climate. What is the cause of the pronounced ENSO-related MSLP signature over the Azores? One could infer that the pattern in Fig. 8b represents the spatial expression of the PNA mode in the model atmosphere. In general, simulated wave trains acquire a more zonal orientation than the observed pattern and would tend to spread and shift eastward of the confined Florida pole. Evidence regarding the role of the PNA over the North Atlantic is presented in Nobre and Schukla (1996). Another possible mechanism is the reduction in the strength of the Hadley cell over the Atlantic sector as suggested by Klein et al. (1999). The representation of these two processes is now investigated in the two subsequent sections.

b. The response of the Atlantic Hadley cell to ENSO forcing

We have limited the period of our study to the last 40 winters (1959–98) to construct composite charts from strong El Niño/La Niña events. For simplicity, we have used the time series of the Niño-3 SST index as the basis to select the years for compositing. Eight cases are retained for each ENSO phase. Anomaly charts for the WARM (1966–69–73–83–87–88–92–98) composite are presented in Fig. 10 both for NCEP and GOGA-EM. Latitudinal cross sections at 25°W (along the Azores–Iceland line) as a function of altitude are displayed for meridional wind and geopotential height fields, both giving a complementary insight into the Hadley cell activity. Comparisons between NCEP and GOGA-EM should call for caution and should be limited to spatial features. Indeed, the averaging process be-

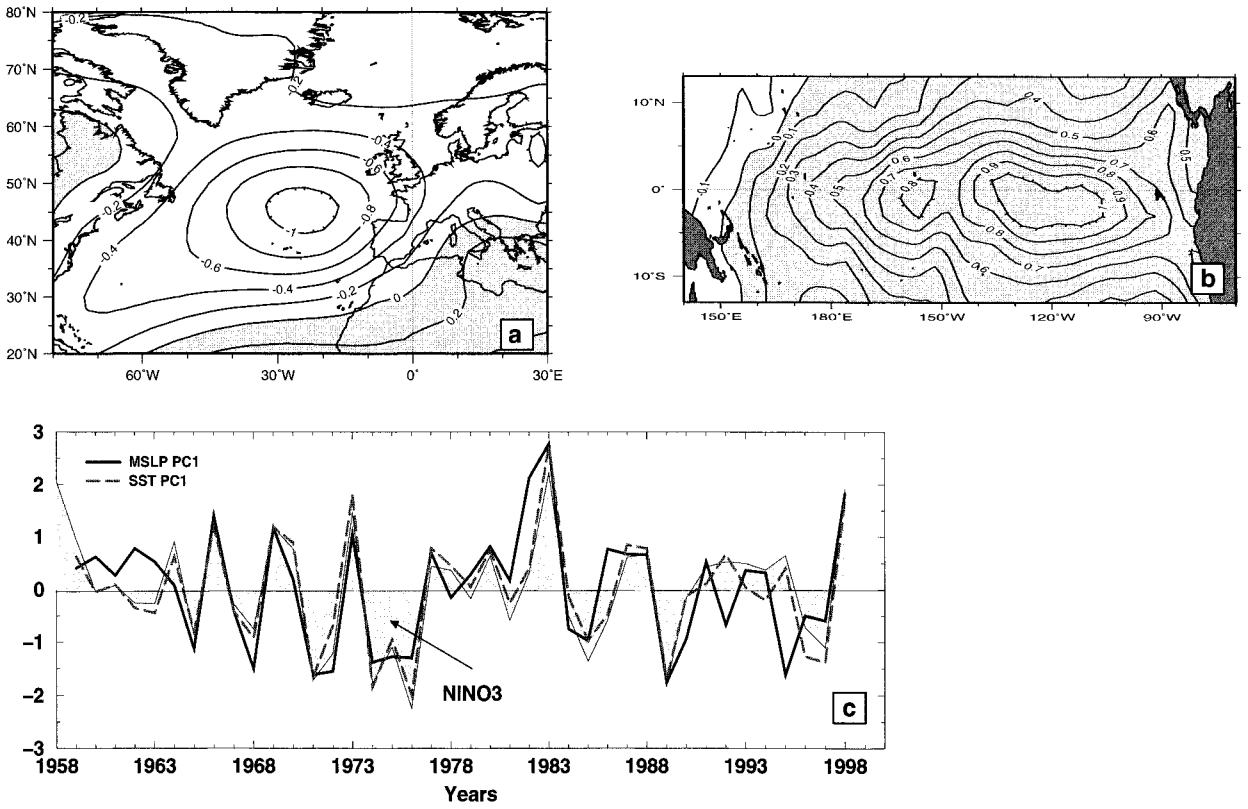

FIG. 8. (a) Homogeneous leading SVD modes of DJF MSLP over the North Atlantic domain from the GOGA-EM experiment and (b) GISST DJF equatorial Pacific SST. Units are hPa and °C with contour intervals equal to 0.2 hPa and 0.1°C, respectively. (c) Normalized associated principal components superimposed on the Niño-3 SST index time series.

tween the individual GOGA simulations filters out a large part of the atmospheric variability.

The composites for NCEP and GOGA-EM share several common characteristics. The sign convention adopted for meridional wind is such that negative anomalies correspond to below-normal northward wind and vice versa. Figure 10a exhibits a notable decrease of the northward upper-troposphere (200–300 hPa) transport both in the model and NCEP from the equator up to 30°N. Positive anomalies from the surface up to 600

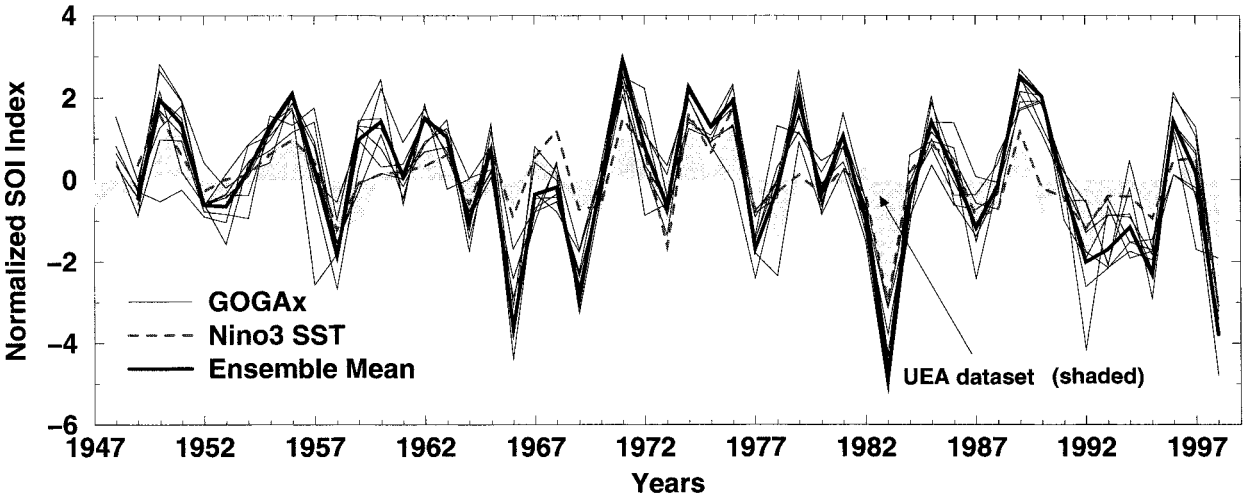

FIG. 9. Time series of the normalized DJF SOI from the UEA dataset (gray shading), each GOGA-type experiment (thin line), the 8-member ensemble mean (heavy solid), and the Niño-3 SST index from 1948 to 1998.

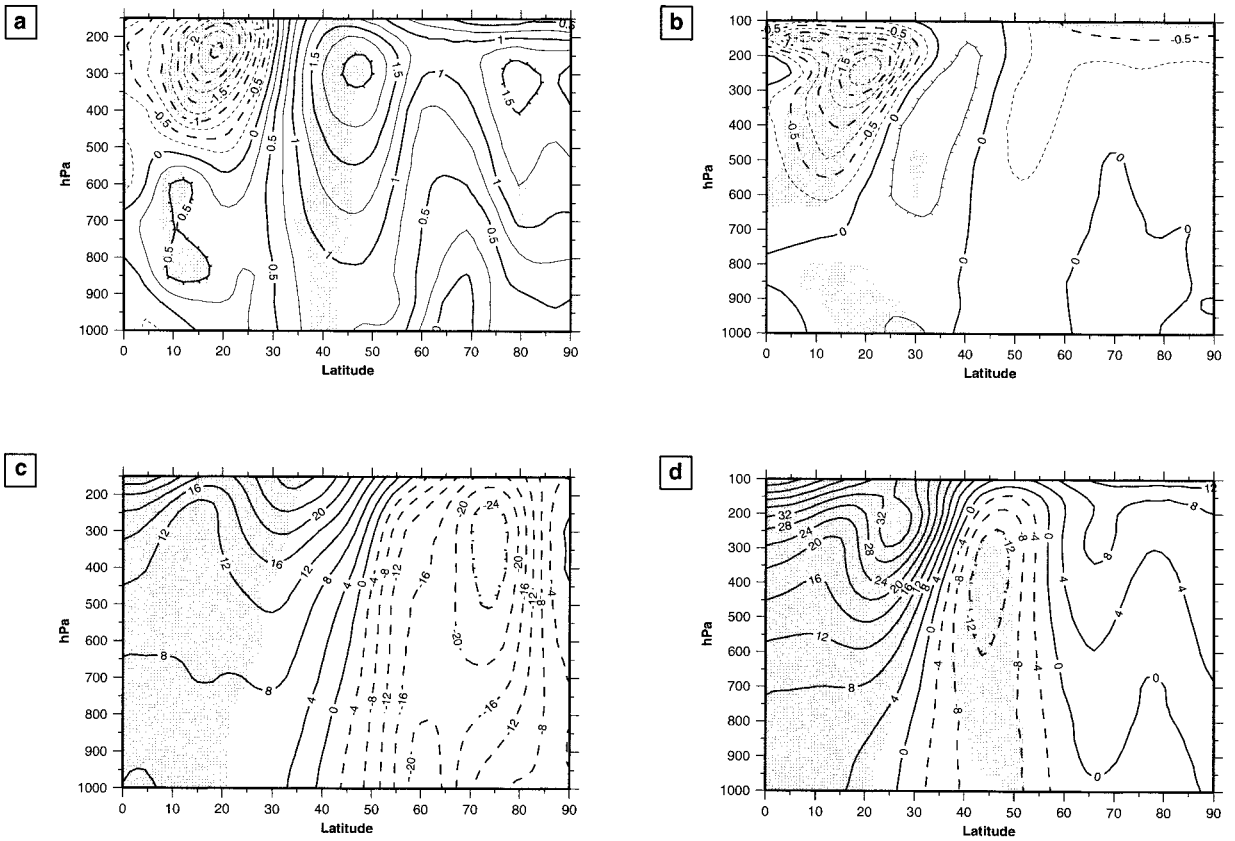

FIG. 10. (a), (b) Meridional wind and (c), (d) geopotential height vertical section at 25°W from the equator to the North Pole obtained by compositing El Niño years. Shading indicates significant anomalies, based on both a two-tailed *t* test and *F* test; (a), (c) are computed for NCEP, (b), (d) represent GOGA-EM results.

hPa and between 10° and 30°N are consistent with reduced trade winds. A sign reversal takes place above the subtropical high (45°N) in NCEP the maximum values occurring at 300 hPa with some continuity over the entire atmospheric column. A similar meridional dipolar structure is apparent in the model but areas of significance are rather limited, the dispersion in the composite between all the Niño years at such a latitude being rather high. The opposition between upper and lower troposphere from the equator to the Tropics (30°N) is suggestive of a weakening of the Hadley circulation and meridional heat transport associated, a finding supported by observational studies (Klein et al. 1999). The ''observed'' anomaly pattern between 35° and 60°N could find its origin in higher latitude, linked for instance to the strength of the Ferrel cell or internal atmospheric processes that dominate regions north of 40°N (see ANOVA conclusions in section 4).

Geopotential height anomalies are depicted in Figs. 10c,d. Comparison between NCEP and GOGA-EM pattern south of 30°N reveals structural similarity. The most significant departure is the emergence in GOGA-EM of a distinct equivalent barotropic negative anomaly between 35° and 55°N. Falling heights above the subtropical high are consistent with a slackened Hadley cell and results on surface fields obtained by SVD analysis, but do not find their counterpart in NCEP that exhibits a much broader negative anomaly north of 40°N. Note that the latter fails at the 95% significance level and it is therefore difficult to draw any conclusions outside of the tropical band. On the other hand, the model results up to 60°N are fairly robust and show a weak dispersion within the composite.

The degree of nonlinearity of the atmosphere response to warm/cold events is fairly high for the meridional wind field in NCEP. Comparison with ''cold composites'' (not shown) reveals opposite anomalous dipolar structure but much weaker amplitude between 40° and 50°N. The model cross section shows a simple sign reversal without magnitude change. Regarding the geopotential height, rather symmetrical behaviors are found both in NCEP and in the model up to 30°N. Beyond these latitudes, NCEP cold composites reveal no significant signal. Model cold composites display the same barotropic signal over the Azores with positive values exceeding 18 m around 400 hPa.

The model results confirm the ENSO influence over the tropical Atlantic via the Hadley cell activity. The

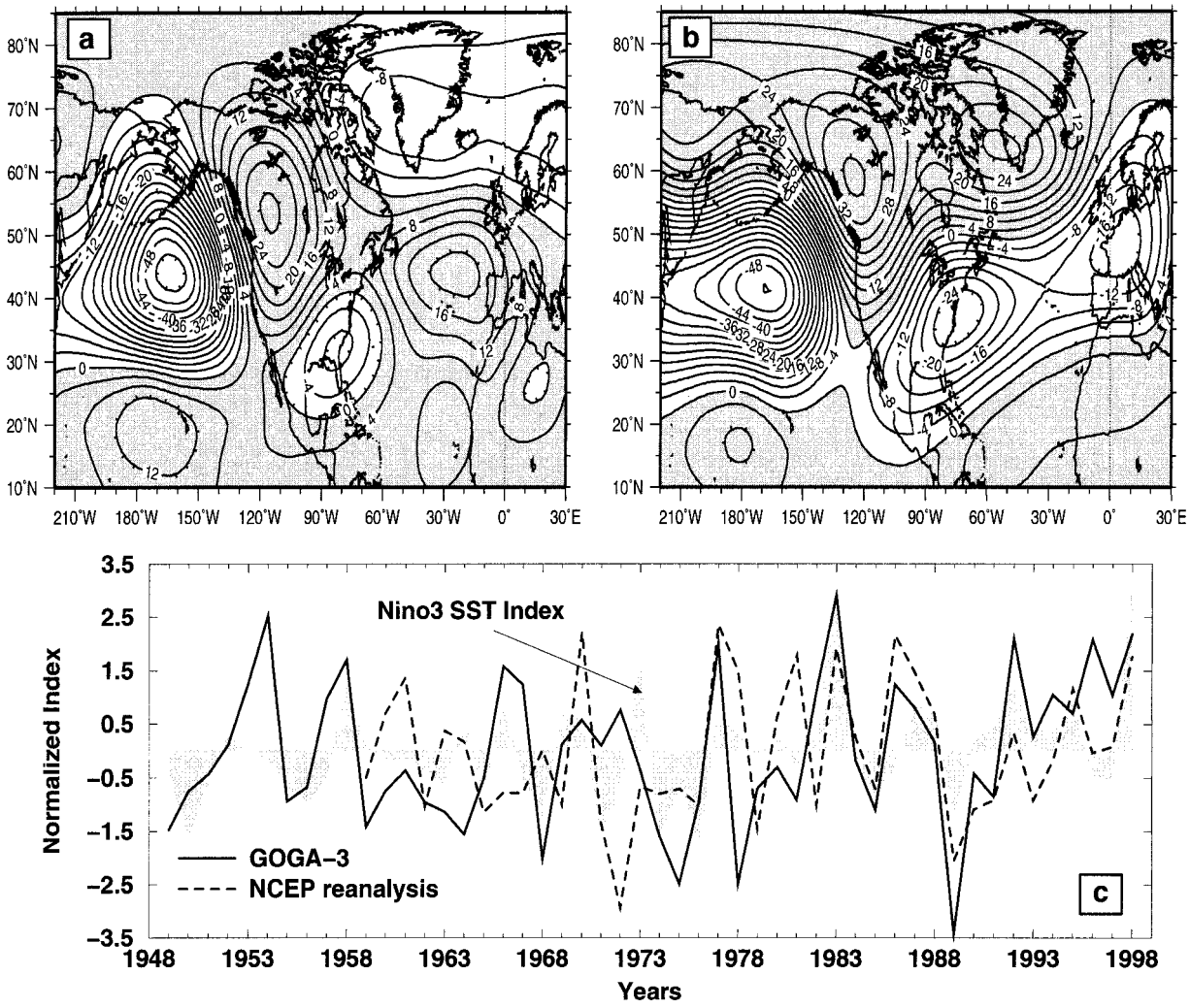

FIG. 11. EOF spatial pattern of the temporal covariance matrix winter 500-hPa geopotential height over the NPA–NAE sector for (a) NCEP EOF2, (b) GOGA EOF1. (c) The Niño-3 SST index and the associated principal components for NCEP and GOGA-3.

main impact is found over the Azores without any significant signature north of 60°N as seen in spectra (IL index). The nearly equivalent barotropic signature suggests that the midlatitude teleconnection patterns characterized by such a vertical structure (Hsu and Wallace 1985) may play an important role and interfere with the Hadley cell response. This is now investigated in the following section.

c. PNA structure and impact over the NAE sector

In analogy with Fig. 5 for the Atlantic sector, the spatial distribution and time evolution of the EOF corresponding to the PNA pattern is examined in Fig. 11. The decomposition is carried out for the 500-hPa geopotential height (Z500) over a larger domain including both the Pacific–American and Atlantic–Europe sectors. NCEP reanalysis and given GOGA EOF patterns are compared. Again spatial modes presented here for ARPEGE are not dependent on the choice of the GOGA experiment.

The PNA mode as defined in Wallace and Gutzler (1981) is captured by the second EOF for NCEP accounting for 18% of the variance. The wavelike appearance characterized by four well-defined centers of action over the Pacific and the North American continent (Hawaï, Gulf of Alaska, Canada, and the southeast United States) exhibits also two secondary poles over the North Atlantic Ocean. These resemble the pressure pattern associated with the NAO suggesting a phase relationship between both teleconnections. In fact, the NAO is captured by the leading EOF mode explaining 22% of the total variance (not shown) that does not show any coherent signal over the NPA sector. The regionalization of the PNA pattern and its separation with the NAO is clearer applying rotation to the

EOF decomposition. Indeed the quadripolar Z500 structure over the NPA domain appears to be very stable whereas the Atlantic dipole amplitude is considerably diminished.

Over the Pacific and the North American continent, the model captures rather well the PNA centers both in terms of amplitude and location. The main discrepency between NCEP and GOGA shows up over the Atlantic with the simulated anomaly centered over the southeast United States now extending farther eastward to western Europe concurrent with a secondary maximum of opposite sign over the Labrador Sea. The Atlantic feature is reminiscent of the Z500 signature of the NAO mode and is not sensitive to rotation. The preferred variability mode over the NPA sector in the ARPEGE model thus tightly links the Pacific and the Atlantic Oceans and reveals a privileged hemispheric-like structure. This mode represents about 40% of the total explained variance namely twice more than NCEP. It is worth noting though that the NAO-like structure associated with the Pacific dynamics in the model is about 1.5 times weaker than the NAO mode obtained when the domain for EOF calculation is restrained to the NAE sector.

We proceed to evaluate the extent to which observed and modeled PNA is linked to ENSO variability. By applying a variety of statistical analyses either linear (EOF, SVD, correlation. . .) (see, e.g., Graham et al. 1994; Lau 1997; Blackmon et al. 1983) or nonlinear (composites, clusters. . .) (e.g., Lau and Nath 1994; Terray and Cassou 2000), many studies have described the remote response of the winter circulation of the Pacific–North America region to SST/diabatic heating anomalies in the central and eastern equatorial Pacific. Robertson and Ghil (1999) showed that the so-called Tropical North hemisphere mode is excited by ENSO. Horel and Wallace (1981) suggested a preference for a PNA-type pattern but a variety of extratropical response during El Niño/La Niña events interacting with the internal atmospheric dynamics are likely to occur thus perturbing the occurrence of the PNA as displayed in Fig. 11c. The correlation coefficient between the Niño-3 index and either the PNA index defined like in Wallace and Gutzler (1981) or the expansion coefficient associated with NCEP EOF2 is rather high (0.43 and 0.51, respectively) but masks interdecadal modulation of ENSO teleconnection as highlighted in Gershunov and Barnett (1998). The last two decades reveal temporal coherence between positive phases of the PNA and ENSO warm events contrasting with the 1960s and 1970s. In the model, the association turns out to be stronger over the entire period. The correlation coefficient between the Niño-3 SST and the GOGA-EM PNA indices reaches 0.67. The power spectrum exhibits a well significant peak around 3.7 yr in agreement with the Niño-3 index one (not shown). It is worth recalling here that comparing GOGA-EM with NCEP values is not directly feasible since the averaging process has removed a large part of the internal variability of the atmosphere that is still present in NCEP. However comparisons between the separated GOGA members still show a tighter link between the PNA mode and ENSO since correlation values ranges from 0.51 to 0.69 among the eight experiments.

This EOF decomposition indicates that the Southern Oscillation has a significant influence in modulating the North Atlantic model variability via the extension of the PNA pattern toward Europe. In the model, negative (positive) phases of the NAO tend to be favored during El Niño (La Niña) events with maximum signature found in the subtropical band. This overestimated ENSO impact may potentially affect the model skill over Europe. Many factors can be responsible for such a bias. The wave train simulation is known to be highly sensitive to the orographic representation and may thus require a finer horizontal and vertical resolution. Another possibility may lie in the representation of the midlatitude transient eddies that are influenced by the stationary waves and in turn have a feedback on their fluctuations. Hoerling and Ting (1994) emphasize the dominant role of anomalous transients in maintaining the extratropical wave train in the Pacific during El Niño/La Niña events. The signature of the simulated atmospheric eddies over the North Atlantic in conjunction with ENSO fluctuations is now examined.

d. Role of the North Atlantic transients in the ENSO–NAE connections

Theoretical studies have shown that midlatitude storm tracks respond to the modified extratropical large-scale circulation perturbed by anomalous tropical heating distribution (Hoskins and Karoly 1981; Branstator 1992). Anomalous storm activity in turn forces the anomalous extratropical wave train, thus providing a positive feedback as demonstrated for instance in Branstator (1995) (see section 3c). This feedback from high- to low-frequency disturbances is examined in Figs. 12a,b showing composite charts of the horizontal component of the **E**-vector divergence calculated respectively on NCEP and individual GOGA experiments (their average being presented here) from 2.2- to 6-day bandpass-filtered fields at 200 hPa. Winter (DJF) daily averages used in constructing these composites were selected on the basis of the winter Niño-3 SST index and for the sake of simplicity, only El Niño composite charts (same years as in section 6b) are displayed. The sign convention adopted for eddy–mean flow interactions is such that positive anomalies correspond to above-normal **E** divergence indicating that the transients are reinforcing the time mean flow. Figures 12a,b highlight the model ability to reproduce the primary features associated with El Niño over the Pacific. In general, the spatial structure of the GOGA-EM response bear a strong resemblance to NCEP with enhanced storminess and transient retroaction off California. Again, weaker amplitudes should be referred to the averaging process between the GOGA

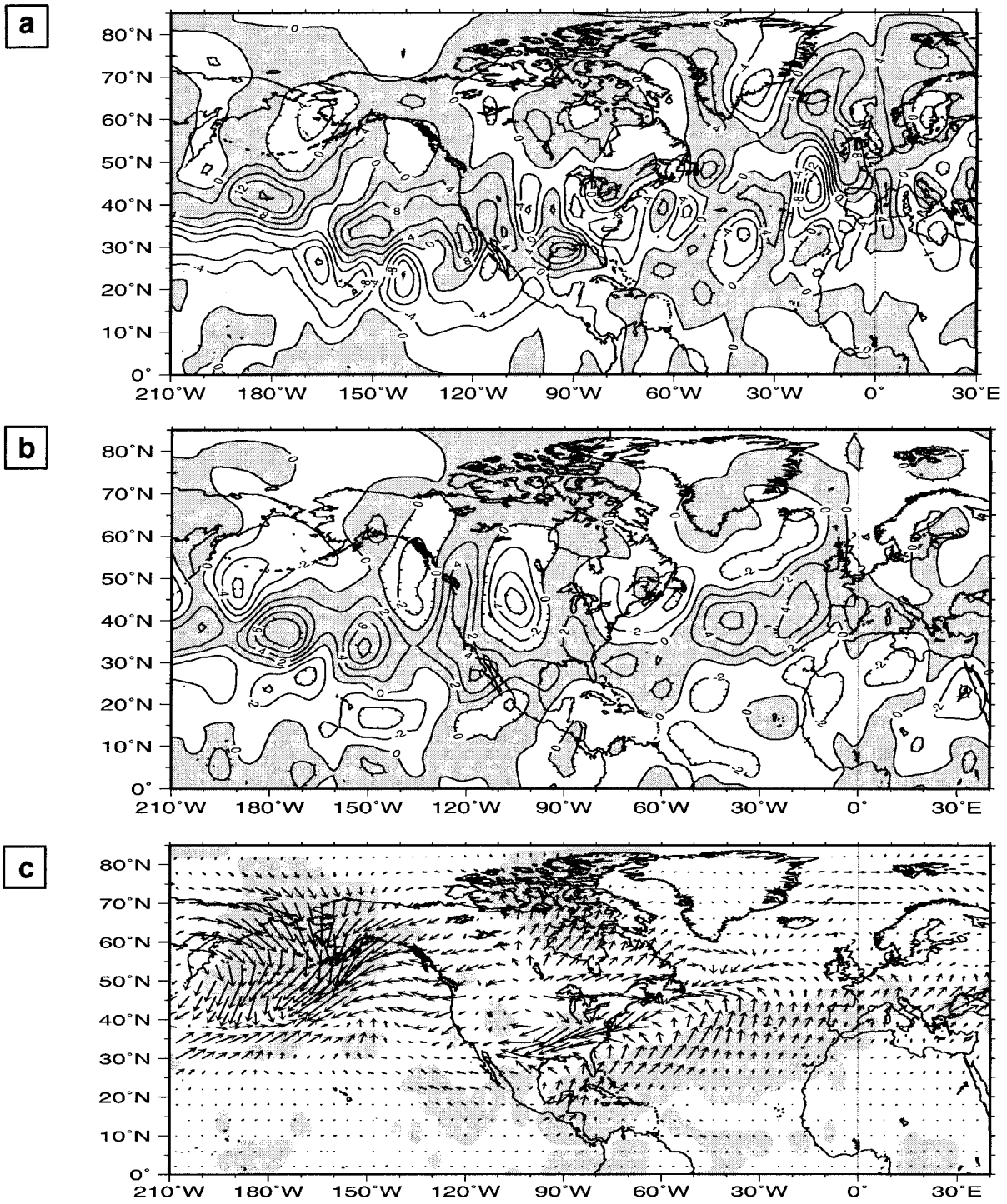

FIG. 12. El Niño winter composites of the **E** horizontal vector divergence computed from 2.2- to 6-day bandpass-filtered daily 200-hPa data from (a) NCEP and (b) from each individual GOGA experiment, their average being presented here. (Note that the contour interval for NCEP is twice the one for GOGA.) (c) El Niño winter composites for $\overline{\mathbf{v}'T'}$ eddy heat transport at 700 hPa, shading stands for significant anomalies using both a two-tailed *t* test and *F* test.

members. Less agreement is found over the North Atlantic. In the model, a band of enhanced divergence extends from Bermuda to France, flanked by zonally elongated anomalous convergence areas. The eastward extension of the PNA trough from Florida is associated with a southward displacement of the Atlantic subtropical jet and a reduction of the northward tilt of its tail. Figure 12b reveals the positive feedback played by transients in order to maintain the PNA extension, therefore contributing to the model bias.

The 700-hPa $\mathbf{v}'\overline{T'}$ composite for warm events calculated on wind and temperature bandpass-filtered fields is displayed for the model only, in Fig. 12c using a vectorial format. Concurrent with the southeastward shift of the Aleutian low and related eastward extension of the subtropical jet, reduced northward eddy heat transport covers a large northern bound of the Pacific Ocean (Bering Strait, Alaska, easternmost tip of Siberia) extending southward in the central basin. Barely significant increased heat transport appears along the jet stream path at about 35°N. The most significant feature shows up in the Atlantic Ocean with a broad area of enhanced northward eddy heat transport from the Caribbean Islands to Spain. This is consistent with enhanced storminess and the southward shift of the main Atlantic storm track in conjunction with the PNA extension along this route. The humidity transport (not shown) by eddies toward southern and western Europe explains excess rainfall over the continent. Note however that whereas the dispersion is rather weak within the model composites, it is very strong in NCEP. Some El Niño years do show a pronounced PNA extension and modified storm activity over the entire Atlantic basin. This is especially true for the 1997–98 warm events where Z500 anomalies over the Azores reach −30 m and ensure the link with the southeastern U.S. PNA pole.

The model behavior is in good agreement with the possible mechanism suggested by Fraedrich (1994) over the NAE region. He postulated that a small alteration of the upstream (west Atlantic) atmospheric circulation due to the PNA could affect the entire North Atlantic cyclogenesis. Positive feedbacks between mean flow and eddy thus play a central role in amplifying and then maintaining geopotential height anomalies downstream to the AH. This mechanism is dominant in the model where the feedbacks involving transients over the eastern Atlantic are strong, in conjunction with the overestimated PNA extension. Comparisons between observed and simulated U200 climatology (see Fig. 2) indicate biases over areas of maximum **E** anomalous divergence during ENSO warm events. The dominance of the ENSO–NAE connection via the transients may thus be partly explained by the model's natural tendency to overestimate the storminess west of Europe. The presence of climatological enhanced synoptic transients over the AH may thus act as a ''bridge'' for the anomalous cycloning forcing from the southeastern United States to western Europe. The misrepresentation of the U200 and baroclinicity mean state privileges the PNA extension that exists in nature only for strong warm (1998) or cold (1989) ENSO events. The credibility of the interference between the simulated climatology and the simulated variability is confirmed by results obtained for the spring season. We have subjected the model outputs averaged over MAM, to the same composite and EOF analyses performed so far in DJF. The MAM PNA pattern does not extend too far westward and is close to the observed mode. This is because the U200 and associated baroclinicity errors are diminished by half over Europe and are now limited over Spain and France. Therefore the MAM mean state is less favorable for an interaction with the transients. The dispersion within the MAM model composites is much stronger than in DJF. The importance of the ''Fraedrich'' mechanism is clearly diminished as it shows up only during strong events (1973–83–98) but disappears for weak to moderate El Niños.

To sum up, it has been shown in this study that the model tends to overestimate the ENSO connections (though realistic in terms of physics) during winter over the NAE sector via the PNA extension and the transients influence ensuring its maintenance. This tendency is shared by numerous AGCMs (Achutarao et al. 2000). The strong ENSO influence may hide the other oceanic forcings whose roles are not negligeable. Figure 7 has shown that Atlantic SSTs also contribute to the NAE atmosphere variability. The competition between those and ENSO is now briefly investigated in the last section.

7. Atlantic SST relationships with the NAE atmosphere

In this chapter, we focus on the relationship between the entire Atlantic SSTs and the North Atlantic MSLP field. Complementary analyses carried out on the 850- and 200-hPa wind will be discussed at the end of the section. Similarly to section 5, SVD techniques are applied between DJF SST and GOGA-EM MSLP detrended datasets. The SST domain extends from 40°S to 75°N limited to the Atlantic (ATL) while the MSLP area is restricted to the North Atlantic (NA) basin, Europe excluded (20°–80°N, 85°W–0°). Indeed, it is found that the SVD results are sensitive to the choice of the atmospheric domain. Including Europe gives different covarying modes and suggests that mecanisms affecting the continent may not be entirely connected to the ones governing the atmospheric flow over the North Atlantic Ocean.

The leading MSLP–SST pair captures 51% of the total square covariance with the second mode accounting for most of the reminder (36%). The basic statistics of the two leading SVD modes are summarized in Table 2. The model MSLP and the GISST SST first modes are displayed, respectively, in Figs. 13a and 13b. The pressure pattern exhibits a monopole centered north of the Azores and is reminiscent of the mode given in Fig.

TABLE 2. Summary of SVD statistics performed over the NA region in winter (DJF) for the MSLP field either the ENSO or the entire Atlantic basin SST domain. Squared Covariance Fraction (SCF), explained variance and coupling correlation coefficient are displayed for modes 1 and 2. Correlation between the principal components associated with the SVD modes and the Niño-3, NATL, and SATL GISST indices are given for both modes. Boldface stands for significant value based on *t*-test statistics.

Winter DJF 1959–98	SCF		Explained variance				Coupling corr coefficient		Correlation with observed SST indices					
	Mode 1	Mode 2	MSLP mode 1	SST mode 1	MSLP mode 2	SST mode 2	Mode 1	Mode 2	Niño-3 mode 1	Niño-3 mode 2	SATL mode 1	SATL mode 2	NATL mode 1	NATL mode 2
NAE–Niño	94	—	8	72	—	—	0.71	—	**0.86**	—	—	—	—	—
NA–ATL	51	36	10	19	28	7	0.65	0.55	**0.63**	0.26	**0.35**	0.01	0.31	**0.42**

8a demonstrated to be associated with ENSO. The SST pattern is basinwide with positive anomalies almost everywhere and maximum warming along the western North African coast and the equatorial band. This structure suggests an interpretation in terms of ENSO connections as illustrated in Enfield and Mayer (1997). The spatiotemporal behavior of this oceanic mode also resembles the 3.5-yr oscillation depicted in Tourre et al. (1999) that cautiously argues its association with ENSO. It mostly finds its origin via the so-called atmospheric bridge mechanism (Klein et al. 1999; Lau 1997) and the modification of the global Walker cell during ENSO.

The second SVD pressure (Fig. 14a) mode captures the NAO with a node located around 50°N and pressure maxima well pined over the climatological centers of action. Comparable anomalies affect both the IL and the AH. The expansion coefficient paired with the pressure mode is well correlated with the model NAOI (0.75). Similarly, maximum energy concentration is found in a broad spectral band centered around 5 yr. The SST covarying pattern (Fig. 14b) exhibits weak anomalies over the entire basin, except in the southern Atlantic off the Uruguayien coasts and tiny coastal zones, off the United States and in the North Sea. The North tropical band is the unique area covered by a large-scale negative anomalies reaching 0.2°C. This pattern can be referred to the classic North Atlantic SST tripole (see, for instance, Cayan 1992). It is close to the one obtained in Rodwell et al. (1999) that presents its relationship with the HadAM NAO mode. The SST principal component shows maximum energy concentration between 4 and 5 yr (Fig. 14c). In agreement with some previous studies, this dominant 4–5-yr peak seems to be linked to both tropical South and tropical North Atlantic SST anomalies. Venegas et al. (1997) find spectral coherence around 5 yr between the DJF South Atlantic MSLP anomalies covarying with the underlying SSTs and the winter NAO index. Rasmusson and Arkin (1993) also evoke a possible relationship between both tropical North and South Atlantic SST and the extratropical teleconnection over the NAE sector with a recurrent 5-yr period. As seen in Table 2, the unique significant correlation value between the pressure PC and the SST indices defined as in Enfield (1996) is found for the North Atlantic index (NATLI) (6°–22°N, 80°–15°W). The latter is further used to suggest a possible mechanism explaining part of the NA response to tropical North Atlantic SST fluctuations.

The model response to the tropical north oceanic conditions is assessed by regressing the two component of the DJF low-level wind at 850 hPa onto the NATLI (Fig. 15a). Warm (cold) SST anomalies over the tropical North Atlantic are associated with a cyclonic (anticyclonic) geostrophic circulation with reduced (enhanced) westerlies around 50°N and reduced trade winds south of the AH. This is the typical NAO-type wind signal in agreement with Venske et al.'s (1999) analyses that sug-

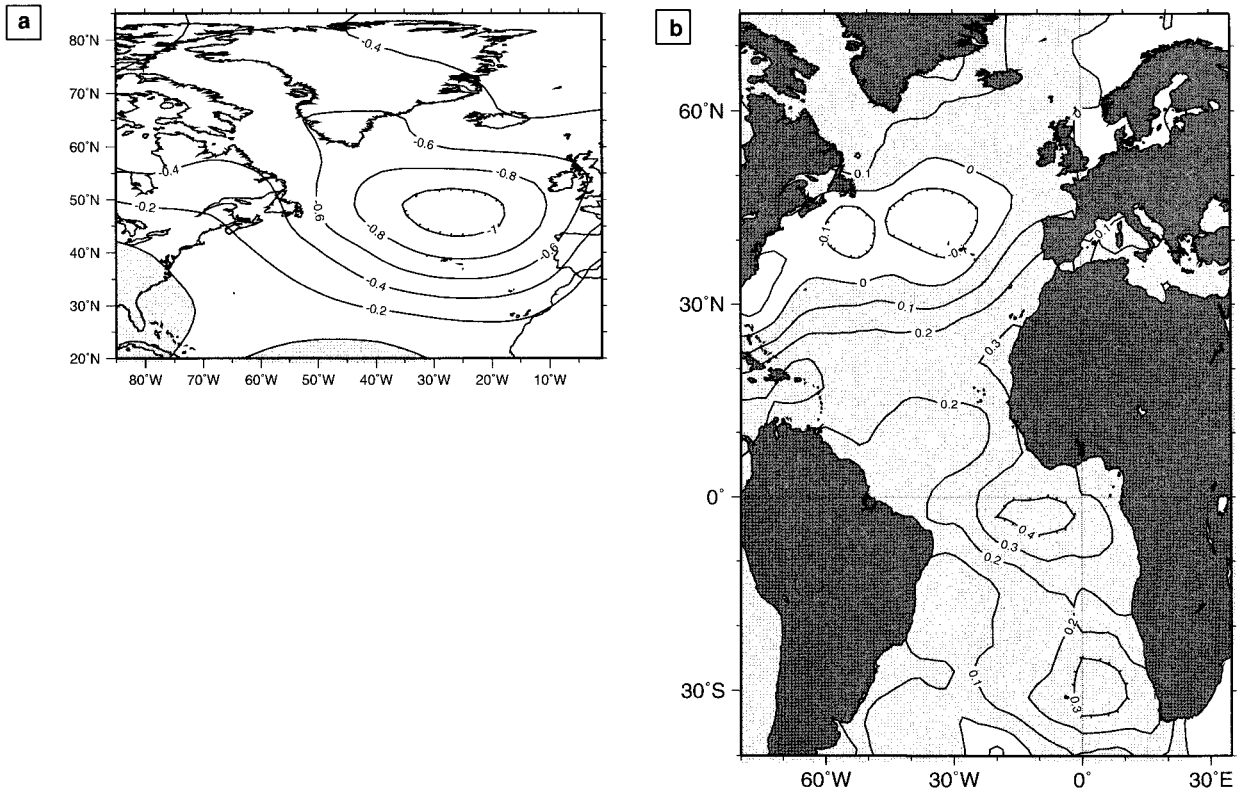

FIG. 13. (a) Homogeneous leading SVD modes of DJF MSLP over the North Atlantic domain from the GOGA-EM experiment and (b) GISST DJF Atlantic SST. Units are hPa and °C with contour intervals equal to 0.2 hPa and 0.1°C, respectively.

gest the dominant impact of the tropical North Atlantic basin.

The linear regression between NATLI and the U200 divergence is presented in Fig. 15b. The U200 wind itself is regressed onto the same index and superimposed. Warm tropical north SST anomalies are related to enhanced divergence over northeast Brazil, the Amazonian basin, and central American countries with concurrent convergence off the Saharian coast around 35°W and above Florida. The U200 is found to be reinforced along the 30°N latitudinal belt with maximum value downstream the anomalous convergence zone over the southeastern United States. The concomitant features between the wind and its divergence suggest a possible mechanism based on local Hadley cell theories as described in Tyrrell et al. (1996) or Rasmusson and Mo (1993) for the Pacific. Enhanced divergence over the South American convective zone reinforces the western local Hadley cell with a stronger sinking branch over Florida. The associated momentum convergence provides an effective Rossby wave forcing as it occurs along the climatological subtropical jet (Sardeshmukh and Hoskins 1988). This leads to the acceleration of the downstream westerlies duct extending up to the central basin, thus creating vorticity anomalies along its flanks that finally affects the AH. The importance of the South America convection zone over land and its connection with the North Atlantic flow has been recently commented in Gedney and Valdes (2000).

The evidence of the tropical North Atlantic influence is difficult to assess through the GOGA experiments alone since changes in the Hadley cell activity may result from different SST domains. Robertson et al. (2000) have shown that the South Atlantic SST fluctuations are related to North Atlantic atmospheric anomalies based on the same Amazonian convection mechanism that would thus ensure an interhemispheric connection. Convergence over Florida is affected by the PNA teleconnection mode and ENSO. GOGA experiments exhibit therefore an integrated response and a key issue would be to quantify the importance of each SST-related contributions as well as their interactions that are supposed to be highly nonlinear. In view of such conclusions, complementary experiments are in progress prescribing SST anomalies over some specific oceanic areas, the rest of the oceans being set to their climatological values.

8. Conclusions and perspectives

a. Summary

In this paper, we focus on a timescale ranging from 2 to 10 yr, trying to identify SST signals over the global

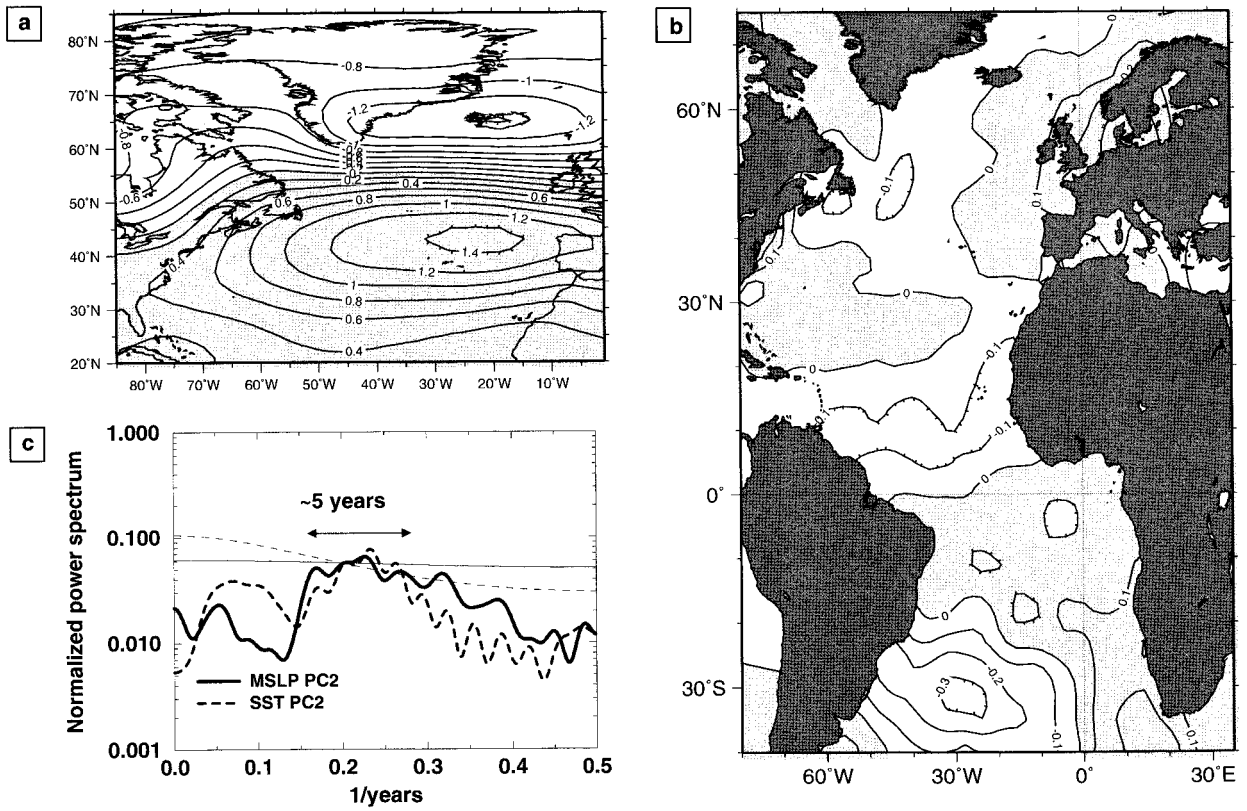

FIG. 14. (a) Homogeneous second SVD modes of DJF MSLP over the North Atlantic domain from the GOGA-EM experiment and (b) GISST DJF Atlantic SST. Units are hPa and °C with contour intervals equal to 0.2 hPa and 0.1°C, respectively. (c) Spectrum of the related expansion coefficients.

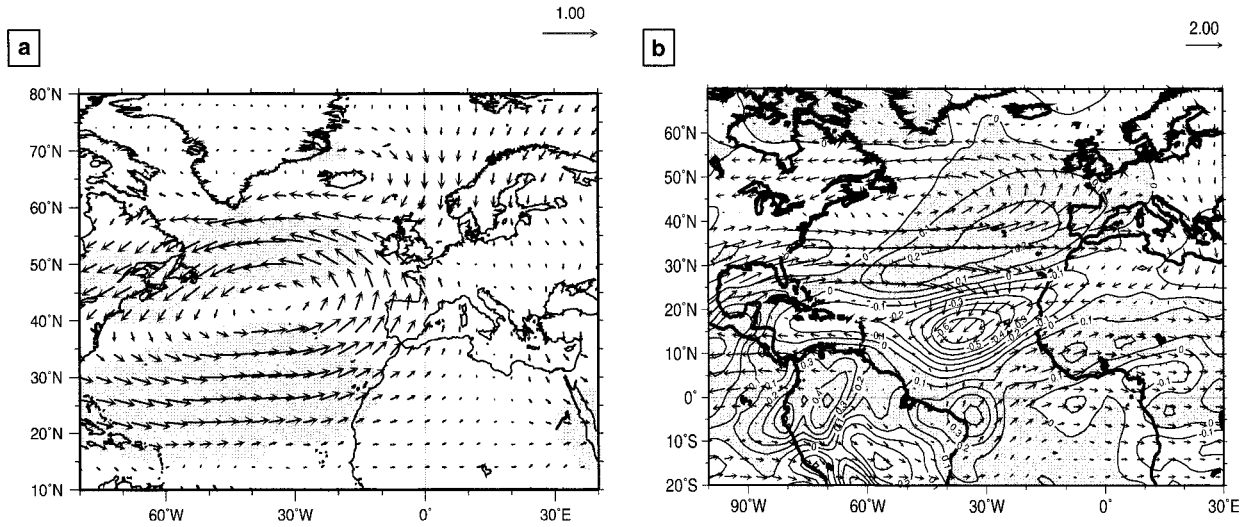

FIG. 15. (a) Regression of the time series of the observed DJF NATLI onto the model wind at 850 hPa. Shading stands for areas above the 95% significance limit based on a *t* test. (b) Regression of the time series of the observed DJF NATLI onto the model upper-tropospheric divergence and 200-hPa wind.

ocean, which are strongly associated with the North Atlantic atmospheric circulation. We conduct this study by examining the behavior of the ARPEGE AGCM forced by prescribed SSTs over the last 50 yr (1948–97). An ensemble of eight simulations was carried out, each member differing by their initial conditions as well as a 60-yr control run forced with (seasonally varying) climatological SSTs. The model was first validated in terms of climatology following by a detailed investigation of the variability over the North Atlantic sector. The realism of results and conclusions is assessed through detailed comparisons to observations or NCEP reanalyses.

At sea level, the model reproduces the basic climatological patterns of the pressure field rather well. Over the Northern Hemisphere, MSLP errors occur primarily during winter where simulated highs over the central Pacific and Atlantic Oceans are too strong while erroneously low pressures are most notable over Europe. Regional discrepancies are found in the mid- to upper-troposphere flow, broadly consistent with the MSLP bias. The eastward extension of the 200-hPa westerly jet over Europe is associated with zonally elongated storm tracks penetrating too far inland. In the Pacific, the northward shift of the main storm path is related to the enhanced subtropical high due to the overestimated Pacific Hadley cell.

The ANOVA method allows us to separate internal (unpredictable) versus SST-forced signals from the total variability. The model develops maximum SST-forced variability over the NAE region in winter and spring although with a weak signal-to-noise ratio. For DJF MSLP, there are weak but significant potential predictability over the Icelandic low and Azores high while the signal is marginal in between. In spring, potential predictability maxima occur over the southeastern United States as well as over the Azores and the southern tip of Europe. Not surprisingly, the highest predictability covers most of the tropical oceans independent of the season. Secondary peaks tend to develop in areas known to be strongly influenced by ENSO via teleconnection or atmospheric bridge processes (NPA sector for instance). Maximum predictive skill of the model is found in winter and spring over the NAE sector but is rather weak.

As this paper deals primarily with the midlatitude Atlantic atmospheric variability, the NAO is investigated using several statistical tools with the aim of highlighting its links with SST anomalies fluctuations. A simple MSLP index that depicts the seesaw NAO-like mode is defined for GOGA-EM. Correlation with observed NAO time series is rather weak and the associated power spectrum reveals two signals with peaks above the 95% confidence limit at periods of 3.7 yr and around 5 yr.

The 3.5-yr peak is related to ENSO dynamics of which influence is restrained to the Azores high. The linkage between climate conditions in the equatorial eastern Pacific and the North Pacific atmospheric circulation represents the archetypal teleconnection that is well captured in the model over the entire NPA sector. ENSO events are associated with trough and ridge structures referred to as the PNA pattern that affects also the westernmost part of the North Atlantic. This study has shown that the winter PNA pattern extends too far eastward toward Europe in the ARPEGE model, which significantly enhances the ENSO connections over the entire NAE region. Transient eddy–mean flow interactions provide a strong feedback that amplifies the original bias. The erroneous PNA extension covers areas where the U200 climatology is not realistic and interactions between mean state and variability are suggested. Indeed, the PNA mode in spring shows a more realistic shape over the Pacific–Atlantic Oceans with reduced extension toward Europe, while the dynamics is better reproduced. Finally ENSO remotely influences the Azores high through the modification of the local Atlantic Hadley cell that is correctly represented in the model.

The most covarying oceanic–atmospheric pattern besides ENSO-related ones, links the NAO to the North Atlantic tripole and exhibits a 5-yr period. A mechanism based on local Hadley cell theories is suggested to link the tropical Atlantic SST anomalies to the NA climate.

b. Discussion and perspectives

This study has brought some evidence that, although most of the variability of the NAO is likely to be internal at interannual timescales, ARPEGE simulations suggest a weak (15% in winter) but significant component forced by SSTs. SST features associated with the NAE atmospheric circulation have been identified by several conventional analyses and it would be of great interest to test their robustness using optimal filtering methods maximizing the signal-to-noise ratio (Venske et al. 1999). Classification techniques are also very appropriate for such a study and results from both techniques will be presented in a forthcoming paper. Conclusions presented here are limited to the identification of synchroneous linkages between atmospheric and SST variations. Time-lag analyses between the two systems should be introduced in order to assess the potential influences of the SST fluctuations in shaping midlatitude atmospheric variability.

The primarily ENSO influence perturbs the global atmospheric circulation and it is therefore more difficult to detect weaker SST signal coming from the Atlantic Ocean. This dominance seems to be present whatever the model and the method of analyses considered (e.g., Venske et al. 1999). An ensemble of four simulations with month-to-month varying SST over the Atlantic and climatological SST elsewhere, has been completed from 1948 to 1998 to further investigate the Atlantic SST influence, the spurious ENSO connection being here eliminated. A reasonable approach would be to improve

the model itself in particular the representation of the stationary waves. Note also that variability biases often tend to appear in areas where the climatological behavior of the model is rather poor. A realistic mean state is crucial to understand and correctly represent the midlatitude atmospheric response to SST anomalies as described in Peng and Whitaker (1999). This reinforces the fact that efforts should still be put on the improvement of the model's mean state.

Since the midlatitude atmospheric variability is governed by a competition between internal dynamics versus SST forcing as well as their mutual influence, results obtained with AGCMs might be highly model dependent since each model has its own noise level. It is striking that Mehtla et al. (2000) obtained correlation values as high as 0.8 comparing their ensemble mean to observed low-pass-filtered NAO index, whereas the maximum found with the ARPEGE set of experiments hardly peaks around 0.35. This is indicative that the model internal processes are dominating any SST-forced signals, however realistic they may be. This is in agreement with the high level of internal variability simulated in the ACYC experiment that is of the same order of magnitude as the total variability present in NCEP (Fig. 5).

Finally, as suggested in several studies (Barsugli and Battisti 1998; Bladé 1999; Bretherton and Battisti 2000), AGCMs forced by prescribed SSTs might yield misleading conclusions as this experimental setup assumes an infinite heat capacity for the ocean. Simulations with either a fully coupled model or a mixed layer ocean component coupled to an AGCM, have demonstrated the significant impact of oceanic feedbacks leading to enhanced thermal variance and persistence of low-frequency patterns. It is indeed essential to simulate this increased persistence and air–sea interactions accurately in order to understand the interannual climate variability. Fully coupled integrations including all the main climate components are in progress and will be compared to the present results in a forthcoming study.

Acknowledgments. We wish to specially thank Sophie Valcke for her constant help and support and for assistance in model output extraction. Thanks are also due to Marie Drévillon for fruitful discussions. The computation were performed at the Météo France Supercomputer Center in Toulouse, France, on VPP700 and at the IDRIS Center in Paris either on the VPP300 or CRAY C90.

REFERENCES

Achutarao, K., and Coauthors, 2000: El Niño–Southern Oscillation in coupled GCMs. PCMDI Rep. 61, 46 pp.

Barnston, A. G., and R. E. Livezey, 1987: Classification, seasonality and persistence of low frequency atmospheric circulation patterns. *Mon. Wea. Rev.,* **115,** 1083–1126.

Barsugli, J. J., and D. S. Battisti, 1998: The basic effects of atmosphere–ocean thermal coupling on midlatitude variability. *J. Atmos. Sci.,* **55,** 477–493.

Bjerknes, J., 1964: Atlantic air–sea interactions. *Advances in Geophysics,* Vol. 10, Academic Press, 1–82.

Blackmon, M. L., J. E. Geisler, and E. J. Pitcher, 1983: A general circulation model study of January climate anomaly patterns associated with interannual variation of equatorial Pacific sea surface temperature. *J. Atmos. Sci.,* **40,** 1410–1425.

Bladé, I., 1997: The influence of midlatitude ocean–atmosphere coupling on the low-frequency variability of a GCM. Part I: No tropical SST forcing. *J. Climate,* **10,** 2087–2106.

——, 1999: The influence of midlatitude ocean–atmosphere coupling on the low-frequency variability of a GCM. Part II: Interannual variability induced by tropical SST forcing. *J. Climate,* **12,** 21–45.

Bougeault, P., 1985: A simple parameterization of the large scale effects of deep cumulus convection. *Mon. Wea. Rev.,* **113,** 2108–2121.

Brankovic, C., T. N. Palmer, and L. Ferranti, 1994: Predictability of seasonal atmospheric variations. *J. Climate,* **7,** 217–237.

Branstator, G., 1992: The maintenance of low-frequency atmospheric anomalies. *J. Atmos. Sci.,* **49,** 1924–1945.

——, 1995: Organization of storm track anomalies by recurring low-frequency circulation anomalies. *J. Atmos. Sci.,* **52,** 207–226.

Bretherton, C. S., and D. S. Battisti, 2000: An interpretation of the results from atmospheric general circulation models forced by the time history of the observed sea surface temperature distribution. *Geophys. Res. Lett.,* **27,** 767–770.

——, C. Smith, and J. M. Wallace, 1992: An intercomparison of methods for finding coupled patterns in climate data. *J. Climate,* **5,** 541–560.

Cassou, C., 1999: A reference validation atlas for the ARPEGE-Climat Version 3 GOGA-type Climatology. Tech. Rep. TR/CMGC/9904, 106 pp.

Cayan, D. R., 1992: Latent and sensible heat flux anomalies over the northern oceans: Driving the sea surface temperature. *J. Phys. Oceanogr.,* **22,** 859–881.

Czaja, A., and C. Frankignoul, 1999: Influence of the North Atlantic SST on the atmospheric circulation. *Geophys. Res. Lett.,* **26,** 2969–2972.

Davies, J. R., D. P. Rowell, and C. K. Folland, 1997: North Atlantic and European seasonal predictability using an ensemble of multidecadal AGCM simulations. *Int. J. Climatol.,* **17,** 1263–1284.

Déqué, M., C. Dreveton, A. Braun, and D. Cariolle, 1994: The climate version of the ARPEGE/IFS: A contribution to the french community climate modelling. *Climate Dyn.,* **10,** 249–266.

Deser, C., and J. M. Wallace, 1990: Large-scale atmospheric circulation features of warm and cold episodes in the tropical Pacific. *J. Climate,* **3,** 1254–1281.

——, and M. L. Blackmon, 1993: Surface climate variations over the North Atlantic Ocean during winter: 1900–1989. *J. Climate,* **6,** 1743–1753.

Douville, H., 1998: Validation and sensitivity of the global hydrological budget in stand-alone simulations with the ISBA land surface scheme. *Climate Dyn.,* **14,** 151–171.

Enfield, D. B., 1996: Relationships of inter-America rainfall to tropical Atlantic and Pacific SST variability. *Geophys. Res. Lett.,* **23,** 3305–3308.

——, and D. A. Mayer, 1997: Tropical Atlantic SST variability and its relation to El Niño Southern Oscillation. *J. Geophys. Res.,* **102,** 929–945.

Fraedrich, K., 1994: ENSO impact over Europe? A review. *Tellus,* **46A,** 541–552.

Frankignoul, C., 1985: Sea surface temperature anomalies, planetery waves, and air–sea feedback in the middle latitudes. *Rev. Geophys.,* **23,** 357–390.

——, A. Czaja, and B. L'Heveder, 1998: Air–sea feedback in the North Atlantic and surface boundary conditions for ocean models. *J. Climate,* **11,** 2310–2324.

Gedney, N., and P. J. Valdes, 2000: The effect of Amazonian defor-

estation on the Northern Hemisphere circulation and climate. *Geophys. Res. Lett.,* **27,** 3053–3056.
Gershunov, A., and T. B. Barnett, 1998: Interdecadal modulation of ENSO teleconnections. *Bull. Amer. Meteor. Soc.,* **79,** 2715–2725.
Graham, N. E., T. P. Barnett, R. Wilde, M. Ponater, and S. Shubert, 1994: On the role of tropical and midlatitude SSTs in forcing interannual to interdecadal variability in the winter Northern Hemisphere circulation. *J. Climate,* **7,** 1416–1441.
Halpert, M. S., and C. F. Ropelewski, 1992: Surface temperature patterns associated with the Southern Oscillation. *J. Climate,* **5,** 577–593.
Harzallah, A., and R. Sadourny, 1995: Internal versus SST-forced atmospheric variability as simulated by an atmospheric general circulation model. *J. Climate,* **8,** 474–495.
Hoerling, M. P., and M. Ting, 1994: Organization of extratropical transients during El Niño. *J. Climate,* **7,** 745–766.
Horel, J. D., and J. M. Wallace, 1981: Planetary scale atmospheric phenomena associated with the Southern Oscillation. *Mon. Wea. Rev.,* **109,** 813–829.
Hoskins, B. J., and D. J. Karoly, 1981: The steady linear response of a spherical atmosphere to thermal and orographic forcing. *J. Atmos. Sci.,* **38,** 1179–1196.
——, I. N. James, and G. H. White, 1983: The shape, propagation and mean flow interaction of large scale weather systems. *J. Atmos. Sci.,* **40,** 1595–1612.
Houghton, J. T., L. G. Meira Filho, B. A. Callander, N. Harris, A. Kattenberg, and K. Marshall, Eds., 1995: *Climate Change 1995: The Science of Climate Change.* Cambridge University Press, 572 pp.
Hsu, H. H., and J. M. Wallace, 1985: Vertical structure of wintertime teleconnection patterns. *J. Atmos. Sci.,* **42,** 1693–1710.
Huang, J., K. Higushi, and A. Shabbar, 1998: The relationship between the North Atlantic Oscillation and El Niño Southern Oscillation. *Geophys. Res. Lett.,* **25,** 2707–2710.
Hurrell, J. W., 1995: Decadal trends in the North Atlantic Oscillation: Regional temperatures and precipitation. *Science,* **269,** 676–679.
——, 1996: Influence of variations in extra-tropical wintertime teleconnections on Northen Hemisphere temperature. *Geophys. Res. Lett.,* **23,** 665–668.
——, and H. van Loon, 1997: Decadal variations in climate change associated with the North Atlantic Oscillation. *Climate Change,* **36,** 301–326.
——, J. J. Hack, B. A. Boville, D. L. Williamson, and J. T. Kiehl, 1998: The dynamical simulation of the NCAR Community Climate Model Version 3 (CCM3). *J. Climate,* **11,** 1207–1244.
Jones, P. D., T. Jonsson, and D. Wheeler, 1997: Extension to the North Atlantic Oscillation using instrumental pressure observations from Gibraltar and southwest Iceland. *Int. J. Climatol.,* **17,** 1433–1450.
Kalnay, E., and Coauthors, 1996: The NCEP/NCAR 40-Year Reanalysis Project. *Bull. Amer. Meteor. Soc.,* **77,** 437–4721.
Kang, I. S., and N. C. Lau, 1986: Principal mode of atmospheric variability in model atmospheres with and without anomalous sea surface forcing in the tropical Pacific. *J. Atmos. Sci.,* **43,** 2719–2735.
Kiladis, G. N., and H. F. Diaz, 1989: Global climatic anomalies associated with extremes in the Southern Oscillation. *J. Climate,* **2,** 1069–1090.
Klein, S. A., B. J. Soden, and N. C. Lau, 1999: Remote sea surface temperature variations during ENSO: Evidence for tropical atmospheric bridge. *J. Climate,* **12,** 917–932.
Kushnir, Y., and I. M. Held, 1996: Equilibrium atmospheric response to North Atlantic SST anomalies. *J. Climate,* **9,** 1208–1220.
Kwok, R., 2000: Recent changes in Arctic Ocean sea ice motion associated with the North Atlantic Oscillation. *Geophys. Res. Lett.,* **27,** 775–778.
Latif, M., and T. P. Barnett, 1994: Causes of decadal climate variability over the North Pacific and North America. *Science,* **266,** 634–637.
Lau, N. C., 1997: Interactions between global SST anomalies and the midlatitude atmospheric circulation. *Bull. Amer. Meteor. Soc.,* **78,** 21–33.
——, and M. J. Nath, 1990: A general circulation model study of the atmospheric response to extratropical SST anomalies observed in 1950–1979. *J. Climate,* **3,** 965–989.
——, and ——, 1994: A modeling study of the relative role of tropical and extratropical SST anomalies in the variability of the global Atmosphere–Ocean system. *J. Climate,* **7,** 1184–1207.
Livezey, R. E., and T. M. Smith, 1999: Covariability of aspects of North Atlantic climate with global sea surface temperatures on interannual to interdecadal timescales. *J. Climate,* **12,** 289–302.
Louis, J. F., M. Tiedke, and J. F. Geleyn, 1982: A short history of the operational PBL parameterization at ECMWF. *Proc. ECMWF Workshop on Planetary Boundary Layer Parameterization,* Reading, United Kingdom, ECMWF, 59–80.
Mehta, V. M., M. J. Suarez, J. V. Manganello, and T. Delworth, 2000: Oceanic influence on the North Atlantic Oscillation and associated Northern Hemisphere climate variations. 1959–1993. *Geophys. Res. Lett.,* **27,** 121–124.
Mestas-Nuñez, A. M., and D. B. Enfield, 1999: Rotated global modes of non-ENSO sea surface temperature. *J. Climate,* **12,** 2734–2746.
Morcrette, J. J., 1990: Impact of changes to the radiative transfer parameterizations plus cloud optical properties in the ECMWF model. *Mon. Wea. Rev.,* **118,** 847–873.
Moron, V., A. Navarra, M. N. Ward, and E. Roeckner, 1998: Skill and reproductibility of seasonal rainfall patterns in the tropics in ECHAM4 GCM simulations with prescribed SST. *Climate Dyn.,* **14,** 83–100.
Nobre, P., and J. Shukla, 1996: Variations of SST, wind stress, and rainfall over the tropical Atlantic and South America. *J. Climate,* **9,** 2464–2479.
Osborn, T. J., K. R. Briffa, S. F. B. Tett, P. D. Jones, and R. M. Trigo, 1999: Evaluation of the North Atlantic Oscillation as simulated by a coupled climate model. *Climate Dyn.,* **15,** 685–702.
Paeth, H., A. Hense, R. Glowienka-Hense, S. Voss, and U. Cubash, 1999: The North Atlantic Oscillation as an indicator for greenhouse-gas induced regional climate change. *Climate Dyn.,* **15,** 953–960.
Palmer, T. N., and Z. Sun, 1985: A modelling and observational study of the relationship between sea surface temperature in the North West Atlantic and the atmospheric general circulation. *Quart. J. Roy. Meteor. Soc.,* **111,** 947–975.
Peng, S., and J. S. Whitaker, 1999: Mechanisms determining the atmospheric response to midlatitude SST anomalies. *J. Climate,* **12,** 1393–1408.
——, L. A. Mysak, H. Ritchie, J. Derome, and B. Bugas, 1995: The differences between early and midwinter responses to sea surface temperature anomalies in the northwest Atlantic. *J. Climate,* **8,** 137–157.
Perlwitz, J., and H. F. Graf, 1995: The statistical connection between tropospheric and stratospheric circulation of the Northern Hemisphere winter. *J. Climate,* **8,** 2281–2295.
Rasmusson, E. M., and P. A. Arkin, 1993: A global view of large-scale precipitation variability. *J. Climate,* **6,** 1495–1522.
——, and K. Mo, 1993: Linkages between 200-mb tropical and extratropical circulation anomalies during the 1986–1989 ENSO cycle. *J. Climate,* **6,** 595–616.
Rayner, N. A., and Coauthors, 1997: Version 2.2 of the Global Sea-Ice and Sea Surface Temperature data set, 1903–1994. Hadley Centre, UK Met Office, CRTN 74, 21 pp.
Renshaw, A. C., D. P. Rowell, and C. K. Folland, 1998: Wintertime low-frequency weather variability in the North Pacific–American sector 1949–93. *J. Climate,* **11,** 1073–1093.
Ricard, J. L., and J. F. Royer, 1993: A statistical cloud scheme for use in AGCM. *Ann. Geophys.,* **11,** 1095–1115.
Robertson, A. W., and M. Ghil, 1999: Large-scale weather regimes and local climate over the Western United States. *J. Climate,* **12,** 1796–1813.

——, C. R. Mechoso, and Y. J. Kim, 2000: The influence of Atlantic sea surface temperature anomalies on the North Atlantic oscillation. *J. Climate,* **13,** 122–138.

Rodo, X., E. Baert, and F. A. Comin, 1997: Variations in seasonal rainfall in southern Europe during the present century: Relationships with the North Atlantic Oscillation and the El Niño Southern Oscillation. *Climate Dyn.,* **13,** 275–284.

Rodwell, M. J., D. P. Rowell, and C. K. Folland, 1999: Oceanic forcing of the wintertime North Atlantic Oscillation and European climate. *Nature,* **398,** 320–323.

Rogers, J. C., 1984: The association between the North Atlantic oscillation and the Southern Oscillation in the Northern Hemisphere. *Mon. Wea. Rev.,* **112,** 1999–2017.

——, 1990: Patterns of low frequency sea level pressure variability (1899–1986) and associated wave cyclone frequencies. *J. Climate,* **3,** 1364–1379.

Rowell, D. P., C. K. Folland, K. Maskell, and N. Ward, 1995: Variability of summer rainfall over tropical north Africa (1906–92): Observations and modelling. *Quart. J. Roy. Meteor. Soc.,* **121,** 669–704.

Saravanan, R., 1998: Atmospheric low-frequency variability and its relationships to midlatitude SST variability: Studies using the NCAR Climate System model. *J. Climate,* **11,** 1386–1404.

——, and J. C. McWilliams, 1997: Stochasticity and spatial resonance in interdecadal climate fluctuations. *J. Climate,* **10,** 2299–2320.

Sardeshmukh, P. D., and B. J. Hoskins, 1988: The generation of global rotational flow by steady idealized tropical divergence. *J. Atmos. Sci.,* **45,** 1228–1251.

Senazzi, F. H. M., B. Burns, N. H. Lin, and J. K. Schemm, 1996: A GCM study of the teleconnections between the continental climate of Africa and global sea surface temperature anomalies. *J. Climate,* **9,** 2480–2497.

Serreze, M. C., F. Carse, R. G. Barry, and J. C. Rogers, 1997: Icelandic low cyclone activity: Climatological features, linkage to the NAO, and relationships with recent changes in the Northern Hemisphere circulation. *J. Climate,* **10,** 453–464.

Servain, J. M., 1991: Simple climatic indices for the tropical Atlantic Ocean and some applications. *J. Geophys. Res.,* **96,** 15 137–15 146.

Stephenson, D. B., V. Pavan, and R. Bojariu, 2000: Is the North Atlantic Oscillation a random walk? *Int. J. Climatol.,* **20,** 1–18.

Stern, W., and K. Miyakoda, 1995: Feasibility of seasonal forecasts inferred from multiple GCM simulations. *J. Climate,* **8,** 1071–1085.

Terray, L., 1998: Sensitivity of climate drift to atmospheric physical parameterizations in a coupled ocean–atmosphere general circulation model. *J. Climate,* **11,** 1633–1658.

——, and C. Cassou, 2000: Modes of low frequency climate variability and their relationships with land precipitation and surface temperature: application to the Northern Hemisphere Winter climate. *SERRA—Stochastic Environ. Res. Risk Assess.,* **14,** 339–369.

Thompson, D. W. J., and J. M. Wallace, 1998: The Artic Oscillation signature in wintertime geopotential height and temperature fields. *Geophys. Res. Lett.,* **25,** 1297–1300.

Ting, M. F., and M. P. Hoerling, 1993: The dynamics of stationary wave anomalies during the 1986/1987 El Niño. *Climate Dyn.,* **9,** 147–164.

Tourre, Y. M., B. Rajagopalan, and Y. Kushnir, 1999: Dominant patterns of climate variability in the Atlantic Ocean during the last 136 years. *J. Climate,* **12,** 2285–2299.

Trenberth, K. E., G. W. Branstator, D. Karoly, A. Kumar, N. C. Lau, and C. Ropelewski, 1998: Progress during TOGA in understanding and modeling global teleconnections associated with tropical sea surface temperatures. *J. Geophys. Res.,* **103,** 14 291–14 324.

Tyrrell, C. G., D. J. Karoly, and J. L. McBride, 1996: Links between tropical convection and variations of the extratropical circulation during TOGA COARE. *J. Atmos. Sci.,* **53,** 2735–2748.

van Loon, H., and J. C. Rogers, 1978: The seesaw in winter temperature between Greenland and Northern Europe. Part I: General description. *Mon. Wea. Rev.,* **106,** 296–310.

Venegas, S. A., L. A. Mysak, and D. N. Straub, 1997: Atmosphere–ocean coupled variability in the South Atlantic. *J. Climate,* **10,** 2904–2920.

Venske, S., M. R. Allen, R. T. Sutton, and D. P. Rowell, 1999: The atmospheric response over the North Atlantic to decadal changes in sea surface temperature. *J. Climate,* **12,** 2562–2584.

Walker, G. T., 1924: Correlations in seasonal variations of weather. *IX Memo. Ind. Meteor. Dept.,* **24,** 275–332.

Wallace, J. M., and D. Gutzler, 1981: Teleconnections in the geopotential height fields during the Northern Hemisphere winter. *Mon. Wea. Rev.,* **109,** 784–812.

——, S. Smith, and C. S. Bertherlon, 1992: Singular value decomposition of wintertime sea surface temperature and 500-mb height anomalies. *J. Climate,* **5,** 561–576.

Ward, M. N., and A. Navarra, 1997: Pattern analysis of SST forced variability in ensemble GCM simulations: Examples over Europe and the tropical Pacific. *J. Climate,* **10,** 2210–2220.

Wunsch, C., 1999: The interpretation of short climate records, with comments on the North Atlantic and Southern Oscillation. *Bull. Amer. Meteor. Soc.,* **80,** 245–255.

Zwiers, F. W., 1987: A potential predictability study conducted with an Atmospheric General Circulation Model. *Mon. Wea. Rev.,* **115,** 2957–2974.

——, 1996: Interannual variability and predictability in an ensemble of AMIP climate simulations conducted with the CCC GCM2. *Climate Dyn.,* **12,** 825–848.